Myeloid HDAC7 drives liver inflammation and systemic glucose dysregulation during diet-induced obesity

Yizhuo Wang[1,2], Divya Ramnath[1,2], Kaustav Das Gupta[1,2,*], Gregory C. Miller[3,4], Prakrithi Pavitra[1,5], Zherui Xiong[1,5], Yujun Wan[6], Ellen N. Tejo[7], James E.B. Curson[1,2], Rishika Abrol[1,2], Sahar Keshvari[7], Kimberley S. Gunther[1,2], Zhixuan Loh[1], Jessica A. Engel[5], Christian R. Engwerda[5], Sabrina Sofia Burgener[1,2], Kate Schroder[1,2], David P. Fairlie[1,2], Andrew D. Clouston[3,4], Elizabeth E. Powell[4,5,8], Katharine M. Irvine[7], Mitchell A. Sullivan[7,9,10], Quan Nguyen[1,5], Matthew J. Sweet[1,2,#] and Denuja Karunakaran[1,11,12,†,#]

Affiliations

[1]Institute for Molecular Bioscience, The University of Queensland, Brisbane, Queensland, Australia.

[2]Australian Infectious Diseases Research Centre, The University of Queensland, Brisbane, Queensland, Australia.

[3]Envoi Specialist Pathologists, Brisbane, Queensland, Australia

[4]Faculty of Health, Medicine and Behavioural Sciences, The University of Queensland, Brisbane, Queensland, Australia

[5]QIMR Berghofer Medical Research Institute, Brisbane, Queensland, Australia

[6]Centre for Nutrition and Food Sciences, Queensland Alliance for Agriculture and Food Innovation, The University of Queensland, Brisbane, Queensland, Australia

[7]Mater Research Institute-UQ, Translational Research Institute, Brisbane, Queensland, Australia

[8]Department of Gastroenterology and Hepatology, Princess Alexandra Hospital, Brisbane, Queensland, Australia

[9]Centre for Bioinnovation and School of Health, University of the Sunshine Coast, Sippy Downs, Queensland, Australia

[10]Sunshine Coast Health Institute, Birtinya, Queensland, Australia

[11]Department of Physiology, Monash Biomedicine Discovery Institute, Monash University, Melbourne, Australia.

[12]Victorian Heart Institute, Victorian Heart Hospital, Melbourne, Australia.

[*]Present address: Division of Infectious Disease, The Lundquist Institute for Biomedical Innovation at Harbor-University of California, Los Angeles Medical Center, Torrance, California, USA.

[†]Present address: Department of Physiology, Monash Biomedicine Discovery Institute, Monash University, Melbourne, Australia

[#]Address correspondence to Matthew J Sweet: m.sweet@imb.uq.edu.au or Denuja Karunakaran: denuja.karunakaran@monash.edu

Abstract

Objectives: Histone deacetylase 7 (HDAC7), a member of the classical HDAC family, promotes LPS-inducible glycolysis and inflammatory mediator production in macrophages, innate immune cells that contribute to pathology in metabolic diseases. Here, we investigated myeloid HDAC7 functions in obesity-driven metabolic disease.

Methods: We used gain- and loss-of-function genetic approaches in mice to investigate myeloid HDAC7 functions in hepatic inflammation and metabolic disease, as well as associations with hepatic gene signatures characteristic of advanced chronic liver disease (CLD).

Results: Transgenic expression of *Hdac7* in myeloid cells increased liver inflammation and liver mRNA levels of *Ccl2* and *Il1b*, key inflammatory mediators linked to CLD. Liver glycogen levels were also decreased, another feature of CLD. Transgenic expression of *Hdac7* in myeloid cells mimicked the hepatic inflammatory phenotype that was observed in mice fed a high fat, high cholesterol, and high sucrose (HFHCHS) diet, an obesity model that mimics some features of metabolic dysfunction-associated steatotic liver disease. In myeloid *Hdac7* transgenic mice fed a HFHCHS diet, weight gain was increased, fasted glucose levels were elevated and glucose tolerance was dysregulated by comparison to control mice. Conversely, fasted blood glucose levels were reduced and glucose tolerance was improved in myeloid *Hdac7*-deleted mice on a HFHCHS diet. *HDAC7* mRNA levels were also elevated in the livers of people with advanced CLD and spatial transcriptomics revealed that myeloid HDAC7 directs hepatic gene signatures characteristic of advanced CLD.

Conclusion: Myeloid HDAC7 contributes to hepatic inflammation and systemic glucose dysregulation in a mouse model of obesity and liver inflammation.

Keywords: glucose metabolism; histone deacetylase 7; inflammation; macrophages; metabolic dysfunction-associated steatotic liver disease; obesity

Introduction

Metabolic dysfunction-associated steatotic liver disease (MASLD) is a common cause of chronic liver disease (CLD) that is associated with substantial morbidity and mortality[1]. MASLD progressing to metabolic-associated steatohepatitis (MASH) is the major cause of cirrhosis, especially in developed countries[2]. MASLD represents a spectrum of conditions, ranging from fatty liver (steatosis) without significant inflammation to MASH, where liver injury, inflammation, and/or fibrosis accompany steatosis[3]. The thyroid hormone receptor-β agonist Resmetirom is approved in the USA as a therapy for patients with moderate to advanced liver fibrosis[4], with other therapies currently under clinical evaluation[5]. For example, the GLP-1 receptor agonist tirzepatide[6] and the bile acid analogue obeticholic acid[7] have shown some promise in reducing scarring in MASH-associated liver fibrosis in phase 2 and 3 clinical trials, respectively. However, these therapies are likely to be effective in only a sub-set of MASH patients. The development of more effective treatments requires a better understanding of the complex underlying mechanisms that drive MASH and the employment of approaches that target multiple inflammatory and fibrotic pathways.

Macrophages are key innate immune cells that sense and respond to endogenous and exogenous danger signals, enabling them to detect perturbations in homeostasis[8]. These cells are extremely heterogeneous, exhibiting diverse phenotypes depending on the specific environmental conditions encountered[9]. Liver macrophages, comprising both tissue-resident Kupffer cells and monocyte-derived macrophages, play important roles in liver homeostasis and in responding to environmental signals. Kupffer cells clear endotoxin and phagocytose bacterial pathogens, dying cells and other debris in the hepatic parenchyma[10-11], and also release inflammatory cytokines upon activation via the pattern recognition receptors, such as toll-like receptor (TLR) 4[12]. Recruited monocytes can also differentiate into macrophages in the liver, either promoting wound healing and tissue repair when the injury-inducing agents have been removed[13-14] or perpetuating inflammation and pathology during active disease[15-16]. A failure to resolve macrophage activation leads to dysregulated production of inflammatory mediators that contribute to pathological conditions, including liver fibrosis[10]. For example, elevated TNF levels in inflamed livers contribute to fibrogenesis[17], the chemokine CCL2 promotes lipid accumulation in hepatocytes leading to obesity-induced liver steatosis[18] and MASH progression[19], and inflammasome-mediated IL-1β production is associated with collagen deposition in MASH patients[20]. Targeting of such inflammatory mediators can attenuate progression of liver disease in mouse models. For example, inhibition of IL-1 receptor

signalling[21] or deletion of *Il1b* that encodes IL-1β[22] in mouse models limited MASH progression.

To fuel proinflammatory responses, aerobic glycolysis is rapidly increased in TLR-activated macrophages[23-24]. This is linked with TCA cycle reprogramming, ultimately resulting in the generation of acetyl-CoA that enables histone modifications for inducible expression of inflammatory genes[25-26]. Signalling molecules that connect glycolysis and inflammation such as the glycolytic enzyme pyruvate kinase isoform 2 (PKM2) have been implicated in the pathogenesis of MASH. For example, elevated levels of PKM2 in both serum and liver were associated with MASLD severity[27]. PKM2 exists in two forms, a tetramer that is associated with its glycolytic function and a dimeric form that drives inflammatory responses. Tetrameric PKM2 polarises macrophages towards a regulatory or anti-inflammatory phenotype, ameliorating liver inflammation and steatosis[28]. In contrast, nuclear accumulation of dimeric PKM2 in macrophages was reported to promote macrophage polarisation towards a pro-inflammatory phenotype, leading to MASH pathogenesis[29]. Significantly, a group of proteins called the class IIa histone deacetylases (HDACs) promote dimerization and activation of the pro-inflammatory form of PKM2 in macrophages[30].

HDACs remove an acetyl moiety from the ε-amino group of lysine residues of histones, with this generally associated with repression of gene transcription[31]. However, thousands of non-histone proteins are also regulated by lysine acetylation[32-33], so HDACs control many cellular processes beyond gene expression. Class IIa HDACs are a subfamily of the classical HDACs that share a conserved C-terminal deacetylase domain and a less conserved N-terminus that interacts with a broad range of cellular proteins[34], allowing this family to regulate various biological processes in physiological and pathological conditions (reviewed in[35-36]). One class IIa HDAC with a particularly important function in metabolic and inflammatory processes in macrophages is HDAC7 (reviewed in[37-38]). In human and murine macrophages, HDAC7 orchestrates LPS-induced glycolysis and the production of key inflammatory mediators IL-1β and CCL2[30], two inflammatory mediators associated with MASLD/MASH. Interestingly, HDAC7 primarily functions in macrophages responding to submaximal concentration of LPS[39], suggesting that this class IIa HDAC may be particularly important in driving chronic low-grade inflammation. In contrast, HDAC7 engages the pentose phosphate pathway in macrophages responding to bacterial challenge, with this enabling pathogen destruction and attenuation of inflammation[40]. This highlights a role for HDAC7 in context-dependent danger recognition during inflammation, meaning that predicting its function in different disease

139 settings such as MASLD/MASH is not straightforward. In this study, using myeloid *Hdac7*
140 gain- and loss-of-function mice, we reveal a role for myeloid HDAC7 in liver inflammation
141 and glucose dysregulation in an obesity model that shares some features with MASLD.

142 ## Results

143 **Myeloid *Hdac7* overexpression promotes liver inflammation in mice**

144 We previously showed that HDAC7 drives production of the pro-inflammatory mediators
145 CCL2 and IL-1β in TLR4-activated macrophages[30-39] and that acute LPS-induced systemic
146 inflammation was amplified in MacHDAC7 mice that selectively over-express HDAC7 in
147 myeloid cells[30]. However, whether myeloid HDAC7 drives inflammatory responses and/or
148 pathological changes in the liver has not been examined. To determine if myeloid HDAC7
149 might contribute to chronic and low-grade liver inflammation, we utilised MacHDAC7
150 transgenic mice[30] that overexpress an alternatively spliced, inflammatory form of murine
151 HDAC7 lacking the first 22 amino acids, HDAC7-u[41], in myeloid cells. In MacHDAC7 mice,
152 *Csf1r* promoter elements direct myeloid-specific expression of the transcriptional activator
153 GAL4-VP16, which in turn drives both HDAC7-u and cyan fluorescent protein (CFP)
154 expression in myeloid cells. Littermate MacBlue mice that express GAL4-VP16-dependent
155 CFP expression were used as controls in these studies[42]. We first evaluated the expression of
156 inflammatory mediators and markers of liver fibrosis in naïve MacBlue and MacHDAC7 mice.
157 As expected, mRNA levels of *Hdac7* were significantly elevated in the livers of MacHDAC7
158 mice compared to those of MacBlue control mice (**Figure 1A**). Thus, the effect of myeloid-
159 specific *Hdac7* overexpression could be detected at the whole-organ level, even in the context
160 of endogenous *Hdac7* expression in hepatocytes and other non-myeloid cells. Consistent with
161 the elevated systemic levels of inflammatory mediators observed upon LPS challenge in
162 MacHDAC7 mice[30], mRNA levels of the inflammatory genes *Ccl2* and *Il1b* were increased in
163 livers of these mice in a basal state (**Figure 1B-C**). Of the fibrotic genes that were examined,
164 only *Mmp9* was increased (**Figure 1D**), with no difference being observed between the two
165 genotypes in mRNA levels of other inflammatory or fibrotic genes such as *Crp*, *Fstl1*, *Col1a1*
166 and *Act2* (**Figure S1**). Thus, myeloid *Hdac7* overexpression increases levels of specific
167 inflammatory mediators in the liver, suggesting that it may prime liver inflammation and/or
168 accelerate liver disease under certain conditions.

169

170 **Myeloid *Hdac7* overexpression increases weight gain in mice fed a HFHCHS diet**

171 To mimic the metabolic and histological changes of MASLD, we placed littermate
172 MacHDAC7 and MacBlue control mice on a HFHCHS diet (20% kcal fat, 20 g/kg cholesterol,
173 222 g/kg fructose and 107 g/kg sucrose) for 24 wk, with weekly body weight gain and
174 metabolic parameters measured. As basal inflammatory mediators were elevated in livers of
175 MacHDAC7 mice (**Figure 1**), cohorts of MacHDAC7 and MacBlue control mice fed on a
176 chow diet were also included. As expected, the HFHCHS diet increased body weight for both

177 genotypes by comparison to their respective chow diet groups. However, weight gain of
178 MacHDAC7 mice fed on either a chow or HFHCHS diet was significantly reduced by
179 comparison to the control MacBlue mice (**Figure 2A**). When correcting for this difference, the
180 weight gain of MacHDAC7 mice on the HFHCHS diet was significantly enhanced over the
181 MacBlue control mice over the 24 wk period of the experiment (**Figure 2B**). To study whole-
182 body metabolism, fat and lean mass was also measured. Interestingly, *Hdac7* overexpression
183 in myeloid cells reduced both the fat and lean mass in mice fed a chow diet (**Figure 2C**, left),
184 consistent with the smaller average body weight of MacHDAC7 mice. This difference was not
185 apparent in mice fed a HCHFHS diet (**Figure 2C**, right), suggesting that this diet increased
186 both fat and lean body compositions in MacHDAC7 mice to a greater extent than MacBlue
187 control mice.
188
189 The HFHCHS diet also significantly increased the weights of liver and epididymal white
190 adipose tissue (WAT) in both MacBlue and MacHDAC7 mice (**Figure 2D-E**) but only
191 MacHDAC7 mice had enlarged kidneys (**Figure 2F**), which may reflect diet-induced renal
192 damage. Interestingly, splenomegaly was observed in the MacHDAC7 mice when fed a chow
193 diet (**Figure 2G**). This suggests perturbed haematopoiesis in the bone marrow environment in
194 these mice, which would be consistent with *Hdac7*-induced liver inflammation in the basal
195 state (**Figure 1**). Collectively, these data demonstrate that overexpression of myeloid *Hdac7*
196 increases diet-induced weight gain.
197
198 **Myeloid *Hdac7* promotes hepatic inflammation but not fibrosis in mice**
199 Given that HDAC7 drives inflammatory responses in primary macrophages[30-39], we postulated
200 that myeloid *Hdac7* overexpression alone may amplify diet-induced liver inflammation. As we
201 previously observed (**Figure 1**), the expression of *Ccl2* and *Il1b* were elevated in MacHDAC7
202 mice fed a chow diet compared to MacBlue control mice (**Figure 3A-B**). Interestingly, this
203 difference was not apparent in mice fed a HFHCHS diet, suggesting that myeloid *Hdac7* alone
204 primed liver inflammation to similar levels triggered by the HFHCHS diet. CCL2 and the
205 accompanying infiltration of inflammatory monocytes contributes to MASH in animal
206 models[43-44]. We therefore assessed circulating CCL2 levels. MacHDAC7 mice fed a chow diet
207 had significantly higher levels of serum CCL2 than the MacBlue control mice (**Figure 3C**).
208 This effect was also apparent in mice fed the HFHCHS diet, although it was less pronounced
209 because the HFHCHS diet increased CCL2 production in only MacBlue mice. Serum IL-1β
210 levels were below the limits of detection in these samples (data not shown), but overall, the
211 results suggest that myeloid *Hdac7* overexpression alone is sufficient to phenocopy hepatic

212 inflammation triggered by the HFHCHS diet. This was confirmed by blinded histological
213 analyses, where liver inflammation was similar between MacHDAC7 mice on a chow diet and
214 MacBlue control mice on a HFHCHS diet (**Figure 3D-E**).
215
216 Having established a role for myeloid HDAC7 in driving liver inflammation, we next assessed
217 its role in liver steatosis and fibrosis. Here we found that the HFHCHS diet induced lipid
218 accumulation and liver steatosis in both MacBlue and MacHDAC7 mice, but this effect was
219 not amplified by *Hdac7* overexpression (**Figure 3F-H**). This suggests that myeloid *Hdac7*
220 overexpression does not have obvious effects on lipid metabolism in the liver. Although
221 histological examination revealed that myeloid *Hdac7* overexpression did not exacerbate
222 HFHCHS-induced liver inflammation (**Figure 3D-E**), we did observe a modest but non-
223 significant increase in NAFLD activity score in MacHDAC7 mice fed a chow diet by
224 comparison to versus MacBlue control mice (**Figure 3I**). However, the HFHCHS diet failed to
225 induce a constant and robust MASH-like phenotype in either group, as shown by the mild and
226 highly variable levels of fibrosis (**Table S1**), thus it remains unclear whether myeloid *Hdac7*
227 promotes diet-induced MASH. Taken together, these observations suggest that myeloid *Hdac7*
228 overexpression promotes hepatic and systemic inflammation, but this alone is not sufficient to
229 drive liver fibrosis.
230
231 **Glucose metabolism is dysregulated in MacHDAC7 mice fed a HFHCHS diet**
232 Insulin resistance is a common metabolic syndrome of MASLD[45]. Thus, we measured fasted
233 blood glucose levels to assess whether myeloid *Hdac7* overexpression regulates hepatic
234 glucose metabolism. When placed on a chow diet, MacHDAC7 mice had consistently lower
235 fasted blood glucose levels than the control MacBlue mice, with these effects being significant
236 at wk 4 and 16 (**Figure 4A**). To assess glucose clearance, we performed intraperitoneal glucose
237 tolerance tests (GTTs) at wk 12, finding that the MacHDAC7 mice cleared injected glucose
238 more rapidly than the MacBlue control, albeit the difference was not statistically significant
239 (**Figure 4B**). However, these phenotypes were reversed when mice were fed a HFHCHS diet,
240 with higher blood glucose levels and slower glucose clearance observed in MacHDAC7 mice
241 (**Figure 4C-D**). This suggests that myeloid HDAC7 has context-dependent roles in regulating
242 glucose metabolism.
243
244 In a fasting state, glucose is mainly produced in the liver via glycogenolysis and
245 gluconeogenesis, with the former converting glycogen into glucose[46]. We therefore considered
246 that hyperglycaemia in the MacHDAC7 mice fed a HFHCHS diet could be due to a change in

247 hepatic glycogen metabolism. Interestingly, MacHDAC7 mice had lower liver glycogen levels
248 than MacBlue control mice when fed the chow diet, with a similar non-significant trend being
249 apparent for mice fed the HFHCHS diet (**Figure 4E**). It is therefore likely that myeloid HDAC7
250 plays a role in glycogen metabolism in both lean and obese mice. Hyperglycaemia inhibits
251 glycogenolysis in healthy individuals, with this inhibition being impaired in type 2 diabetes
252 mellitus[47]. Since MacHDAC7 mice fed a HFHCHS diet had lower hepatic glycogen levels
253 (**Figure 4E**) and increased fasting glucose levels (**Figure 4C**) than MacBlue mice, we propose
254 that regulatory control of hepatic glycogen breakdown may be impaired in MacHDAC7 mice,
255 leading to enhanced glycogenolysis. We conclude that myeloid HDAC7 overexpression
256 exacerbates HFHCHS diet-induced dysregulation of glucose and glycogen metabolism.
257
258 Inflammatory mediators such as CCL2 promote macrophage infiltration, hepatic inflammation,
259 and insulin resistance during diet-induced obesity[48-49]. Considering the role of HDAC7 in
260 macrophage inflammation and that myeloid *Hdac7* expression triggered higher levels of
261 circulating CCL2 (**Figure 3C**), we next wondered whether myeloid *Hdac7* alters insulin
262 secretion during obesity. Indeed, insulin levels were reduced in MacHDAC7 mice versus
263 MacBlue control mice fed a chow diet (**Figure 4F**, centre). This suggests that lean MacHDAC7
264 mice (**Figure 2C**) control insulin levels to respond to their lower blood glucose levels (**Figure**
265 **4A**). Interestingly, when fed a HFHCHS diet, both MacBlue and MacHDAC7 mice had
266 similarly elevated insulin levels (**Figure 4F**, right), suggesting a feedback mechanism of
267 increased insulin production to suppress elevated blood glucose levels. However, these
268 increased insulin levels failed to control glucose production in MacHDAC7 mice (**Figure 4C**).
269 We conclude that elevated HDAC7 expression in myeloid cells drives metabolic dysregulation,
270 a feature of type 2 diabetes mellitus[50].
271
272 **Myeloid *Hdac7* deletion does not alter weight gain but attenuates HFHCHS diet-induced**
273 **glucose dysregulation**
274 Given that myeloid *Hdac7* overexpression triggered inflammation and dysregulated glucose
275 homeostasis in diet-induced obesity, we hypothesised that genetically targeting *Hdac7* in
276 myeloid cells would ameliorate HFHCHS-induced phenotypes. To test this, we used myeloid-
277 restricted *Hdac7*$^{-/-}$ mice (*Hdac7*$^{fl/fl}$ *LysM*^{Cre}) and littermate *Hdac7*$^{+/+}$ control mice (*Hdac7*$^{fl/fl}$),
278 placing the mice on a HFHCHS diet for a period of 36 wk with the goal of inducing more
279 severe MASH phenotypes. In contrast to the enhanced weight gain of myeloid HDAC7 gain-
280 of-function mice (**Figure 2B**), *Hdac7* deletion from myeloid cells did not affect weight gain in
281 mice fed a HFHCHS diet (**Figure S2A**). Similarly, fat and lean mass (**Figure S2B**) and organ

282 weights (**Figure S2C**) were unaffected, although there was a modest trend towards reduced
283 liver mass. These data indicate that myeloid *Hdac7* deficiency does not prevent the
284 development of obesity.
285
286 Next, we examined glucose metabolism to determine whether myeloid *Hdac7* deletion
287 improves the dysregulated phenotypes induced by the HFHCHS diet. *Hdac7*$^{-/-}$ mice had similar
288 blood glucose levels to the control mice at the beginning of the study (**Figure 5A**, 0 wk).
289 However, starting from wk 8 of HFHCHS feeding, myeloid-restricted *Hdac7*$^{-/-}$ mice had
290 consistently lower fasted blood glucose levels than *Hdac7*$^{+/+}$ mice, with the effects being
291 significant at wk 8, 14 and 16 (**Figure 5A**). This suggests that deletion of *Hdac7* from myeloid
292 cells improves blood glucose regulation. This effect was also reflected in improved glucose
293 tolerance in *Hdac7*$^{-/-}$ mice (**Figure 5B-C**). *Hdac7*$^{-/-}$ mice also presented with slightly improved
294 insulin sensitivity than control mice, although these effects were not significant (**Figure 5D-**
295 **E**). Hence, myeloid deletion of *Hdac7* reduces fasting glucose and improves glucose
296 intolerance in the HFHCHS obesity model.
297
298 **Myeloid *Hdac7* deletion did not ameliorate diet-induced hepatic pathology and**
299 **inflammation**
300 Next, we assessed whether the effects of *Hdac7* deletion on glucose metabolism may relate to
301 inflammation. At the cellular level, levels of HDAC7 protein were greatly reduced in bone
302 marrow derived macrophages (BMMs) from *Hdac7*$^{-/-}$ mice fed on both HFHCHS and chow
303 diets, as expected (**Figure S3A**). Consistent with previous findings[30], LPS-inducible CCL2 and
304 inflammasome-triggered IL-1β levels were reduced in BMMs from the naïve *Hdac7*$^{-/-}$ mice on
305 a chow diet (**Figure S3B**, right side of graphs). However, in *Hdac7*$^{-/-}$ BMMs generated from
306 mice fed the HFHCHS diet, only IL-1β levels were significantly reduced, with CCL2 levels
307 being only marginally affected (**Figure S3B**, left side of graphs). These data indicate that the
308 capacity of HDAC7 to drive the production of these inflammatory mediators in macrophages
309 may be attenuated under the conditions of obesity. Consistent with this, hepatic *Ccl2* mRNA
310 levels were only slightly reduced in myeloid *Hdac7*$^{-/-}$ mice (**Figure S3C**). Liver *Il1b* mRNA
311 levels (**Figure S3D**) and circulating CCL2 levels (**Figure S3E**) were also unaffected.
312 Histological assessment of livers from these mice revealed that the HFHCHS diet induced only
313 varying levels of early to moderate stages of liver fibrosis in mice from either genotype (**Figure**
314 **S4A**). Of note, the *Hdac7*$^{-/-}$ mice trended towards a very modest reduction in liver inflammation,
315 lipid accumulation, steatosis and fibrosis compared to the *Hdac7*$^{+/+}$ control mice (**Figure S4B-**
316 **F**). This suggests that myeloid *Hdac7* deletion may very modestly reduce obesity-induced

317 pathological processes in the liver. We conclude that myeloid HDAC7 drives glucose
318 dysregulation but only marginally contributes to hepatic inflammation and fibrosis in the
319 HFHCHS diet model.
320
321 **Myeloid *HDAC7* expression is associated with gene expression signatures linked to**
322 **advanced CLD**
323 Our data support a role for HDAC7 in mediating glucose dysregulation in both gain- and -loss
324 of function mouse models, as well as liver inflammation in a gain-of-function mouse model.
325 We therefore considered that elevated HDAC7 expression in CLD may contribute to metabolic
326 dysregulation and/or disease progression. We thus assessed *HDAC7* mRNA levels in liver
327 biopsies of people with early or advanced CLD[51]. Here we found that *HDAC7* mRNA levels
328 were elevated in livers from people with advanced CLD by comparison to those with early
329 disease (**Figure 6A**), suggestive a link between HDAC7 and human CLD severity. To further
330 investigate this link in myeloid cells, we performed spatial transcriptomic analysis on livers
331 from MacBlue and MacHDAC7 mice fed a chow diet to identify myeloid HDAC7-associated
332 transcriptional changes relevant to CLD. We first identified cells co-expressing *eCFP* and
333 *Hdac7* mRNAs in livers, then performed differential gene expression analysis on
334 *eCFP*$^{+}$/*Hdac7*$^{+}$ cells from MacBlue versus MacHDAC7 mice. A heatmap of the 53
335 differentially expressed genes is shown in **Figure 6B**. This analysis confirmed elevated *Il1b*,
336 *Ccl2* and *Mmp9* mRNA levels in hepatic myeloid cells from MacHDAC7 mice (**Figure 6B**),
337 consistent with our previous findings in whole liver tissue (**Figure 1B-D**). When compared
338 with our previously published dataset of genes associated with early and advanced human
339 CLD[51], we found that eight genes associated with advanced CLD in human were also
340 differentially expressed in *eCFP*$^{+}$ cells in livers of MacHDAC7 mice. These include *Vcan*,
341 *Thbs1*, *Mmp9* and *Rab8b*, several of which have been implicated in CLD progression and/or
342 pathology[52-54]. Spatial co-expression analysis revealed that these genes were co-expressed with
343 HDAC7, with limited expression in other hepatic cells (**Figure 6C-F**). This suggests that
344 myeloid HDAC7 expression is sufficient to direct gene expression programs associated with
345 advanced CLD. In summary, data presented in this study implicate myeloid HDAC7 in driving
346 hepatic inflammation and expression of genes linked to advanced CLD, as well as systemic
347 glucose dysregulation in a mouse obesity model.

348 **Discussion**

349 In this study, we investigated potential roles of myeloid HDAC7 in metabolic diseases,
350 examining obesity, glucose dysregulation, hepatic inflammation and fibrosis. Although levels
351 of steatosis and fibrosis were variable in our studies (**Figure 3F-I, S4C-F, Table S1**), HFHCHS
352 fed mice did develop diet-induced obesity (**Figure 2A**) and liver inflammation (**Figure 3D-E**).
353 We therefore focused our studies on indicators of metabolism and inflammation. We found the
354 overexpression of myeloid *Hdac7* promoted hepatic inflammation in a basal state, mimicking
355 diet-induced liver inflammation and associated pathological changes. Of note, in the HFHCHS
356 diet model, glucose dysregulation was exacerbated in myeloid HDAC7 gain-of-function mice
357 and improved in myeloid HDAC7 loss-of-function mice. These findings thus extend the
358 functions of HDAC7 in macrophages beyond cellular metabolism[30-39-40] to whole body glucose
359 metabolism.
360
361 MacHDAC7 mice on a HFHCHS diet had increased hyperglycaemia at multiple time points
362 (**Figure 4C**), as well as impaired glucose tolerance (**Figure 4D**), by comparison to MacBlue
363 control mice. Conversely, hyperglycaemia (**Figure 5A**) and glucose clearance (**Figure 5B**)
364 were improved in myeloid *Hdac7*$^{-/-}$ mice on a HFHCHS diet. Collectively, these data reveal a
365 role for myeloid HDAC7 in driving glucose dysregulation during obesity. Interestingly,
366 MacHDAC7 mice on a chow diet had reduced levels of fasted blood glucose (**Figure 4A**) and
367 liver glycogen (**Figure 4E**), suggesting that glycogen metabolism is disrupted in these mice.
368 Under fasting conditions, glycogenolysis is initiated by glucagon and epinephrine-dependent
369 cascades[55]. Glycogen phosphorylase is a key enzyme controlling glycogenolysis, converting
370 glycogen to glucose-1-phosphate, which is subsequently converted to glucose-6-phosphate that
371 feeds glycolysis[56]. A previous study found that glycogen phosphorylase activity is controlled
372 by post-translational modifications. Specifically, acetylation at K470 inhibits its enzymatic
373 activity, with this inactivation mechanism being enhanced by insulin[57]. MacHDAC7 mice on
374 the chow diet had significantly lower blood insulin levels than control MacBlue mice, with this
375 difference being absent in mice fed the HFHCHS diet (**Figure 4F**). Thus, myeloid HDAC7
376 may somehow limit insulin secretion in MacHDAC7 mice to indirectly enhance glycogenolysis
377 in hepatic cells. Alternatively, it is also possible that HDAC7 promotes glycogen breakdown
378 in macrophages, which could contribute to glucose dysregulation in the setting of obesity.
379 Activated macrophages have been shown to store glycogen and metabolise it to drive
380 inflammatory responses via multiple mechanisms[58]. Thus, HDAC7-mediated glycogenolysis
381 in macrophages could contribute to both dysregulated inflammation and glucose metabolism
382 during obesity. We previously showed that HDAC7 increases the enzymatic activity of the

383 glycolytic enzyme PKM2 by interacting with it and promoting its deacetylation[30] and it is
384 possible that HDAC7 similarly activates enzymes in the glycogenolysis pathway in
385 macrophages.
386
387 In the fasting state, another source of hepatic glucose production is gluconeogenesis, which is
388 under strict hormonal control. Silencing of HDAC4, 5 and 7 in mouse livers led to higher liver
389 glycogen content and improved glucose tolerance[59]. Mechanistically, the fasting hormone
390 glucagon promotes the dephosphorylation and nuclear shuttling of class IIa HDACs in HepG2
391 hepatocytes. In the nucleus, class IIa HDACs recruit HDAC3 to promoter regions of
392 gluconeogenic genes to enable the deacetylation of the FOXO transcription factor and the
393 induction of downstream genes, including *G6pc* that encodes glucose-6-phosphatase, a key
394 enzyme mediating gluconeogenesis[59]. An analogous pathway of hormone-activated
395 HDAC4/FOXO regulation of glucose and lipid metabolism was also identified in *Drosophila*
396 *melanogaster*[60]. Given these studies, it is possible that myeloid HDAC7 also contributes to
397 hyperglycaemia via activating gluconeogenic genes downstream of glucagon signalling.
398
399 Liver inflammation in MacHDAC7 and MacBlue mice on the HFHCHS was comparable
400 (**Figure 3A-E**). Notably however, the MacHDAC7 mice already exhibited significantly higher
401 liver inflammation in the basal state (**Figure 3A-E**). The lack of an enhanced inflammatory
402 phenotype in obese MacHDAC7 mice may reflect that HDAC7 overexpression phenocopies
403 diet-induced inflammation. In contrast, levels of inflammatory mediators were not significantly
404 reduced in the livers or plasma of myeloid *Hdac7*$^{-/-}$ mice fed a HFHCHS diet (**Figure S3-S4**),
405 although BMMs isolated from these mice on a chow diet showed reduced production of
406 inflammatory mediators (**Figure S3B**, right side of graphs). The lack of an obesity-driven
407 inflammatory phenotype in myeloid *Hdac7*$^{-/-}$ mice may reflect compensatory effect of other
408 class IIa HDACs, as previously observed in activated macrophages *in vitro*[30]. It may also reflect
409 variability in efficiency and/or specificity of the LysM-Cre system for conditional gene
410 deletion in myeloid cells[61], as highlighted by a previous study examining immune and non-
411 immune cell populations of the lung[62]. Alternatively, myeloid HDAC7 may have distinct roles
412 in obesity- versus LPS-driven inflammation. We previously showed that HDAC7 promotes
413 glycolysis and associated IL-1β production in macrophages responding to LPS[30]. However,
414 during bacterial infection, macrophage HDAC7 engages the pentose phosphate pathway to
415 generate the metabolite ribulose-5-phosphate that suppresses macrophage inflammatory
416 responses[40]. This context-dependent role of myeloid HDAC7 in controlling macrophage
417 inflammatory responses makes it difficult to predict its functions in different inflammation-

418 driven conditions. Nonetheless, taken together with the pronounced effects of myeloid gain-
419 of-function HDAC7 in exacerbating hepatic inflammation (**Figure 1, 3**), the subtle reduction
420 in phenotypes associated with MASLD in myeloid *Hdac7*$^{-/-}$ mice (**Figure S4**) suggests that
421 HDAC7 in macrophages contributes to hepatic inflammation during obesity, in addition to its
422 effects in dysregulating metabolism.
423
424 In conclusion, this study has identified an association between myeloid HDAC7 and both
425 hepatic and systemic glucose metabolism, thus identifying a potential role for macrophage-
426 expressed HDAC7 in controlling whole body metabolism. This lysine deacetylase and
427 scaffolding protein likely promotes the breakdown of liver glycogen, which may partly explain
428 HDAC7-mediated hyperglycaemia during obesity. Myeloid HDAC7 overexpression also
429 phenocopied diet-induced liver inflammation in mice, consistent with the known role of
430 HDAC7 in promoting inflammatory responses[30-39-63] and oxidative stress[40] in macrophages.
431 Thus, small molecule inhibitors of class IIa HDACs[64-65] should be evaluated in the future for
432 their capacity to attenuate dysregulated metabolism and/or inflammation in mouse models of
433 obesity-driven CLD. Notably, *HDAC7* expression was elevated in liver biopsies of people with
434 advanced versus early CLD (**Figure 6A**) and in tumours derived from a mouse liver carcinoma
435 model[66], with myeloid HDAC7 directing expression of genes associated with advanced CLD
436 in human (**Figure 6B-F**). Thus, it will also be of interest in the future to explore the
437 involvement of myeloid HDAC7 in obesity-linked liver fibrosis during CLD progression.

438 ## Materials and methods

439 **Ethics statement**

440 All animal studies were approved by The University of Queensland Animal Ethics Committee.
441 Experimental procedures followed the approved projects 2021/AE00629, 2021/AE00630 and
442 2021/AE001048. Mice were bred and housed on a 12 h-controlled day/night cycle with food
443 and water available ad libitum in the Queensland Biosciences Precinct animal house (Institute
444 for Molecular Bioscience, The University of Queensland). Mice were monitored during
445 experiments in accordance with protocols approved in the above animal ethics certificates.
446

447 **Animals**

448 6-10 wk old male MacHDAC7 mice and control MacBlue mice (total of n=14-15 per group)
449 were fed a HFHCHS diet containing 20% kcal fat, 20 g/kg cholesterol, 222 g/kg fructose and
450 107 g/kg sucrose (Specialty Feeds, SF21-160, containing sodium caseinate) for 24 wk. The
451 control groups (n=3 per genotype) were fed a chow diet for the same time. These experiments
452 were carried out as two independent trials. Alternatively, 8-12 wk old male *Hdac7*$^{-/-}$ and wild
453 type control *Hdac7*$^{+/+}$ mice (n=12 per genotype) were fed a HFHCHS diet (Specialty Feeds,
454 SF18-074, same nutrient composition to SF21-160 except that it contains casein) for 36 wk.
455 Body weight was measured weekly throughout the trials. Fat and lean mass was measured
456 using a Minispec LF50 NMR Analyser (Bruker) one week before the end of the study. At the
457 termination of the study, mice were fasted for 6 or 12 h before being euthanised with isoflurane.
458 Blood was collected via cardiac puncture followed by perfusion with 0.9% saline solution
459 (Baxter). Liver, spleen, kidney and epididymal white adipose tissue were collected, weighed,
460 snap frozen, then fixed in 10% neutral buffered formalin or processed for RNA extraction.
461

462 **Fasted glucose measurements**

463 Mice were fasted for 6 h before blood was collected at midday from the saphenous or tail vein
464 using an EDTA-coated collection tube every 4 wk. Glucose levels were measured immediately
465 after the puncture with an Accu-Check Aviva Nano glucose meter (Roche).
466

467 **Glucose and insulin tolerance tests**

468 Mice were fasted for 6 h and blood glucose levels were measured from the tail vein before
469 intraperitoneal injection. For glucose tolerance tests, MacHDAC7 and MacBlue mice were
470 injected with 2 g/kg of D-glucose (AJAX), whereas *Hdac7*$^{-/-}$ and *Hdac7*$^{+/+}$ mice were injected
471 with 1g/kg of glucose. For insulin tolerance tests, *Hdac7*$^{-/-}$ and *Hdac7*$^{+/+}$ mice were fasted for

472 6 h before being injected with 0.75 U/kg insulin (NovoRapid). Blood glucose levels were
473 measured from the tail vein at the indicated time points with an Accu-Check Aviva Nano
474 glucose meter (Roche). For the tests on MacHDAC7 and MacBlue mice, data were combined
475 from two independent experiments.
476
477 **Histological assessment**
478 Formalin-fixed mouse livers were processed for paraffin-embedded histology for Hematoxylin
479 and Eosin (H&E) and Sirius Red staining. Unstained slides were processed for H&E staining
480 using a DAKO autostainer. Sirius Red slides were processed using the Llewellyn modification
481 of the Sirius Red technique[67]. In short, slides were stained with haematoxylin and then treated
482 with Sirius Red solution for 1 h before washing in tap water for 10 min. Slides were imaged
483 using a clinical microscope (BX43 or BX51, Olympus). Livers were scored using the NASH
484 Clinical research Network (NASH-CRN) scoring system[68]. In this method, scores for steatosis,
485 ballooning and lobular inflammation are summed to generate an overall score for likelihood of
486 steatohepatitis.
487
488 **Glycogen quantification**
489 The method used was previously described[69-70]. Snap-frozen mouse livers were homogenised
490 in 1 mL isolation buffer (50 mM Tris, pH 8, 150 mM NaCl, 2 mM EDTA, 50 mM NaF, 5 mM
491 sodium pyrophosphate, Sigma-Aldrich). 20 µL homogenate was then digested in 22.5 µL
492 acetate mix (1:8 mixture of 10% acetic acid (Sigma-Aldrich):200 mM sodium acetate buffer
493 (Sigma-Aldrich) (pH4.5)) with 5 µL and amyloglucosidase ~3260 U/mL, Megazyme) at 50 °C
494 for 30 min. The same amount of undigested liver homogenates boiled for 10 min was used for
495 correcting background glucose levels. Liver homogenates were then centrifuged at 20,000 *g*
496 for 10 min and transferred to a 96-well plate. Serially diluted D-glucose was used for generating
497 the calibration curve. 30 µL samples were then mixed with a reaction mix containing 150 µL
498 of 200 mM tricine/KOH (pH 8) (Sigma-Aldrich) and 10 mM MgCl2 (Sigma-Aldrich), 1 µL of
499 112.5 mM NADP (NADP), 1 µL of 180 mM of ATP (NADP) and 0.5 µL glucose-6-phosphate
500 dehydrogenase (Roche) to a volume of 200 µL. Absorbance at 340 nm was recorded for 20 min
501 before as well as 30 min after the addition of hexokinase (Roche). Glycogen content was
502 corrected for the weight of homogenised liver tissues.
503
504 **Insulin measurements**
505 Blood collected from saphenous vein or by cardiac puncture was centrifuged at 10,000 rpm for
506 10 min. Concentrations of insulin in mouse serum or plasma were measured using a mouse

507 insulin ELISA kit (Crystal Chem Mouse Insulin ELISA Kit, 90080), following the
508 manufacturer's instruction. Standard solutions and samples were added in duplicate into the
509 wells included in the kits and incubated for 2 h at 4 °C . Each well was then washed thoroughly.
510 Next, enzyme conjugate solution was added and incubated for 30 min at room temperature,
511 followed by another washing step. Enzyme substrate solution was immediately added and
512 incubated for 40 mi at room temperature in the dark. Following that, enzyme stop solution was
513 added to each well to stop the reaction. Finally, the absorbance at A450 and A630 was
514 measured using a microplate reader. Sample insulin concentrations were calculated based on a
515 standard curve generated using known insulin concentrations from the standard solutions
516 included in the kits.
517
518 **Cell culture**
519 Bone marrow cells were collected from femurs and tibias of mice and cultured in RPMI media
520 supplemented with 10% FBS, 2mM L-glutamine, 50 U/mL penicillin and 50 µg/mL
521 streptomycin (Gibco) in the presence of 150 ng/mL recombinant human macrophage colony-
522 stimulating factor-1 (Protein Expression Facility, UQ) for 6 days. Differentiated BMMs were
523 harvested in DPBS (Thermo Fisher Scientific) and resuspended in culture media for stimulation
524 with indicated concentrations of LPS (*Salmonella enterica* serotype Minnesota, L2137, Sigma-
525 Aldrich). To induce IL-1β processing and secretion, 5 µg/mL nigericin (N7143, Sigma-Aldrich)
526 was added to cells 1 h prior to harvesting culture supernatants. Cell culture supernatants were
527 then collected, centrifuged at 1,000 *g* for 5 min and stored at -80 °C until analysis.
528
529 **Cytokine profiling**
530 Cell culture supernatants and mouse plasma were diluted in culture media and DPBS,
531 respectively. CCL2 and IL-1β concentrations were measured using MCP-1/CCL2 Mouse
532 Uncoated ELISA and IL-1beta Mouse Uncoated ELISA Kits (mouse CCL2: 88-7391-77,
533 mouse IL-1β: 88-7013-77, Invitrogen) or with a Mouse CCL2/JE/MCP-1 DuoSet ELISA kit
534 (DY479, R&D SYSTEMS), as per the manufacturer's manuals.
535
536 **Quantification of gene expression**
537 To extract RNA from mouse livers, fresh tissues were frozen in lysis buffer from an ISOLATE
538 II RNA Mini kit (BioLine) at -80 °C. Snap-frozen tissues from naïve mice were homogenised
539 in lysis buffer. RNA purification was performed following the manufacturer's instructions. An
540 off-column DNA digestion was performed using DNAse I (Invitrogen), as per manufacturer's
541 instructions. RNA was reverse transcribed to cDNA using oligo dT and SuperScript III Reverse

542 Transcriptase (Invitrogen). Quantitative PCR (qPCR) was performed in 384-well plates using
543 cDNAs, SYBR Green PCR Master Mix (Applied Biosystem), and a ViiATM 7 Real-Time PCR
544 System (Applied Biosystems). mRNA levels of individual genes, relative to the housekeeping
545 gene hypoxanthine phosphoribosyl transferase (*Hprt*), were calculated using the ΔCt method[71].
546 Sequences of primers used for qPCR are listed in **Table S2**.
547
548 **Western blotting**
549 Differentiated BMMs were washed once with DPBS and lysed in RIPA buffer (50 mM Tris-
550 HCl, 150 mM NaCl, 0.1% SDS, 1% Sodium deoxycholate, 1% NP-40) supplemented with
551 protease inhibitor cocktail (cOmpleteTM, Roche) and phosphatase inhibitors (PhosStopTM,
552 Roche). Cell lysates were homogenised by passing through a 27G needle. Equal amounts of
553 homogenates were boiled and subjected to electrophoresis using pre-cast 4-12% Bis-Tris
554 NuPAGE gels in NuPAGE MOPS SDS running buffer (Invitrogen). After separation, proteins
555 were transferred to a nitrocellulose membrane and immunoblotted for endogenous HDAC7
556 using an anti-HDAC7 antibody (Cell Signaling Technology, 1/1000) followed by an HRP-
557 conjugated goat anti-rabbit IgG (Cell Signaling Technology, 0.026 µg/mL) and Tubulin as a
558 loading control using a fluorescent Rhodamine anti-Tubulin antibody (Bio-Rad, 1/5000).
559
560 **Quantification of hepatic *HDAC7* mRNA levels in human CLD**
561 Hepatic *HDAC7* mRNA levels were quantified in a cohort of 69 people with CLD of mixed
562 aetiologies. Diagnosis, disease scoring and sample stratification has previously been
563 described[51]. *HDAC7* mRNA levels in people with early (stages 0-2) and advanced (stages 3-4)
564 CLD were quantified by RNA sequencing, as previously described[51]. In brief, sequencing reads
565 were mapped to the human hg19 genome using STAR aligner[72] and CPM values of transcript
566 reads were obtained using the edgeR package[73]. Genes were filtered with a CPM threshold of
567 over 10 in at least 20 samples and subjected to normalisation using the Trimmed Mean of M-
568 values method using edgeR[74]. Differential gene expression was then analysed by likelihood-
569 ratio test, with multiple testing performed using Benjamini-Hochberg corrections[75]. FDR
570 values of less than 0.05 were considered significantly different.
571
572 **Spatial transcriptomics analyses**
573 Liver tissues were harvested from two male MacBlue and two male MacHDAC7 mice and
574 immediately fixed in 4% paraformaldehyde for 24 h at 4°C. Fixed tissues were processed,
575 embedded in paraffin, and sectioned at 5 µm thickness. Sections were mounted onto Xenium
576 V1 slides (10x Genomics) and processed according to the manufacturer's protocol for Xenium

577 Prime In Situ Gene Expression with Cell Segmentation Staining (10x Genomics, CG000760
578 RevC). Briefly, slides underwent deparaffinization and decrosslinking, followed by priming
579 hybridization, RNase treatment and polishing. The Xenium 5K Ms PTP Panel Probes (10x
580 Genomics, Cat#2001227) and an add-on custom probe panel targeting 50 genes, including key
581 macrophage, inflammatory, metabolic, and fibrosis-associated transcripts, was hybridised to
582 the tissue sections overnight. Following probe ligation, rolling circle amplification and cell
583 segmentation staining steps, slides were loaded onto Xenium Analyzer for signal detection and
584 image acquisition. Raw image data were processed using the Xenium Onboard Analysis
585 pipeline, and decoded transcripts were mapped back to the tissue at the single cell level. Data
586 were analysed using Seurat workflow (Seurat version 5.1.0), including quality control filtering,
587 and gene expression quantification in R (version 4.4.0). EdgeR (version 4.4.0) was used to
588 perform differential gene expression analysis on MacBlue versus MacHDAC7 hepatic cells
589 that were positive for both *eCFP* and *Hdac7* mRNAs and the results were visualised on a
590 heatmap. Genes overlapping with previously published CLD-associated signatures were
591 further examined for spatial co-localisation with bivariate Moran's Index (from esda package
592 version 2.2.1) using custom python scripts and were visualised with spatial feature plots.
593
594 **Statistical analyses**
595 Data from *in vivo* experiments are combined from one or two independent trials with each
596 individual mouse representing one independent data point. For cell culture experiments, means
597 of experimental replicates were determined, with data from independent mice or experiments
598 being combined for statistical analysis. Statistical analyses were performed using Prism 9 or
599 10 (GraphPad). Comparisons between two groups were performed using a two-tailed unpaired
600 Student's *t*-test. For datasets involving at least three variables, linear regression, ordinary or
601 repeated measures two-way ANOVA tests were performed followed by multiple comparisons,
602 as indicated in individual figure legends. Differences with confidence value of 95% and above
603 ($p < 0.05$) were considered statistically significant.

Acknowledgements

This work was supported by a National Health and Medical Research Council of Australia (NHMRC) Ideas grant (1184885 to MJS and DR), an NHMRC Investigator grant to MJS (1194406), and an Australian Infectious Disease Research Centre seed grant to CRE, MJS, JAE and DR. DK was supported by an Institute for Molecular Bioscience (IMB) Fellowship and an NHMRC Ideas grant (2012772). DPF was supported by an NHMRC Investigator grant (2009551) and an ARC Centre of Excellence grant (CE200100012). SSB was supported by a Swiss National Science Foundation Postdoc Mobility Fellowship (P2BEP3_191800) and a Novartis Foundation for Medical-Biological Research Fellowship (21C133). KMI was supported by an NHMRC Ideas grant (2012793).

Author contributions

Conceptualisation, Y.W., M.A.S., M.J.S., D.K.; Methodology, G.C.M., S.K., K.S.G., Z.L., S.S.B., K.M.I; Investigation, Y.W., D.R., K.D.G., G.C.M., P.P., Z.X., Y.W., E.N.T., J.E.B.C., R.A., D.K.; Resources, G.C.M., C.R.E, J.A.E., A.D.C., E.E.P., Q.N.; Writing- original draft, Y.W., M.J.S., D.K.; Writing- Review/Writing, Y.W., G.C.M., P.P., S.S.B., D.P.F., K.M.I., M.A.S., M.J.S., D.K.; Supervision, K.S., D.P.F., A.D.C., K.M.I., M.A.S., Q.N., M.J.S., D.K.; Funding acquisition, D.R., C.R.E, J.A.E., M.J.S.

Conflict of Interest Statement

The authors claim no conflict of interest.

626 **References**

627 1. Huang DQ, Terrault NA, Tacke F, Gluud LL, Arrese M, Bugianesi E, et al. Global
628 epidemiology of cirrhosis - aetiology, trends and predictions. Nat Rev Gastroenterol Hepatol.
629 2023;20(6):388-98.
630 2. Moon AM, Singal AG, Tapper EB. Contemporary Epidemiology of Chronic Liver
631 Disease and Cirrhosis. Clin Gastroenterol Hepatol. 2020;18(12):2650-66.
632 3. Mitra S, De A, Chowdhury A. Epidemiology of non-alcoholic and alcoholic fatty liver
633 diseases. Transl Gastroenterol Hepatol. 2020;5:16.
634 4. Keam SJ. Resmetirom: First Approval. Drugs. 2024;84(6):729-35.
635 5. Harrison SA, Loomba R, Dubourg J, Ratziu V, Noureddin M. Clinical Trial Landscape
636 in NASH. Clin Gastroenterol Hepatol. 2023;21(8):2001-14.
637 6. Loomba R, Hartman ML, Lawitz EJ, Vuppalanchi R, Boursier J, Bugianesi E, et al.
638 Tirzepatide for Metabolic Dysfunction-Associated Steatohepatitis with Liver Fibrosis. N Engl
639 J Med. 2024;391(4):299-310.
640 7. Sanyal AJ, Ratziu V, Loomba R, Anstee QM, Kowdley KV, Rinella ME, et al. Results
641 from a new efficacy and safety analysis of the REGENERATE trial of obeticholic acid for
642 treatment of pre-cirrhotic fibrosis due to non-alcoholic steatohepatitis. J Hepatol.
643 2023;79(5):1110-20.
644 8. Mosser DM, Edwards JP. Exploring the full spectrum of macrophage activation. Nat
645 Rev Immunol. 2008;8(12):958-69.
646 9. Davies LC, Jenkins SJ, Allen JE, Taylor PR. Tissue-resident macrophages. Nat
647 Immunol. 2013;14(10):986-95.
648 10. Nguyen-Lefebvre AT, Horuzsko A. Kupffer Cell Metabolism and Function. J Enzymol
649 Metab. 2015;1(1).
650 11. Dixon LJ, Barnes M, Tang H, Pritchard MT, Nagy LE. Kupffer cells in the liver. Compr
651 Physiol. 2013;3(2):785-97.
652 12. Tosello-Trampont AC, Landes SG, Nguyen V, Novobrantseva TI, Hahn YS. Kuppfer
653 cells trigger nonalcoholic steatohepatitis development in diet-induced mouse model through
654 tumor necrosis factor-alpha production. J Biol Chem. 2012;287(48):40161-72.
655 13. Murray PJ, Wynn TA. Protective and pathogenic functions of macrophage subsets. Nat
656 Rev Immunol. 2011;11(11):723-37.
657 14. Ramachandran P, Pellicoro A, Vernon MA, Boulter L, Aucott RL, Ali A, et al.
658 Differential Ly-6C expression identifies the recruited macrophage phenotype, which

659 orchestrates the regression of murine liver fibrosis. Proc Natl Acad Sci U S A.
660 2012;109(46):E3186-95.
661 15. Obstfeld AE, Sugaru E, Thearle M, Francisco AM, Gayet C, Ginsberg HN, et al. C-C
662 chemokine receptor 2 (CCR2) regulates the hepatic recruitment of myeloid cells that promote
663 obesity-induced hepatic steatosis. Diabetes. 2010;59(4):916-25.
664 16. Rivera CA, Adegboyega P, van Rooijen N, Tagalicud A, Allman M, Wallace M. Toll-
665 like receptor-4 signaling and Kupffer cells play pivotal roles in the pathogenesis of non-
666 alcoholic steatohepatitis. J Hepatol. 2007;47(4):571-9.
667 17. Braunersreuther V, Viviani GL, Mach F, Montecucco F. Role of cytokines and
668 chemokines in non-alcoholic fatty liver disease. World J Gastroenterol. 2012;18(8):727-35.
669 18. Rull A, Rodriguez F, Aragones G, Marsillach J, Beltran R, Alonso-Villaverde C, et al.
670 Hepatic monocyte chemoattractant protein-1 is upregulated by dietary cholesterol and
671 contributes to liver steatosis. Cytokine. 2009;48(3):273-9.
672 19. Haukeland JW, Damas JK, Konopski Z, Loberg EM, Haaland T, Goverud I, et al.
673 Systemic inflammation in nonalcoholic fatty liver disease is characterized by elevated levels
674 of CCL2. J Hepatol. 2006;44(6):1167-74.
675 20. Wree A, McGeough MD, Pena CA, Schlattjan M, Li H, Inzaugarat ME, et al. NLRP3
676 inflammasome activation is required for fibrosis development in NAFLD. J Mol Med (Berl).
677 2014;92(10):1069-82.
678 21. Negrin KA, Roth Flach RJ, DiStefano MT, Matevossian A, Friedline RH, Jung D, et
679 al. IL-1 signaling in obesity-induced hepatic lipogenesis and steatosis. PLoS One.
680 2014;9(9):e107265.
681 22. Kamari Y, Shaish A, Vax E, Shemesh S, Kandel-Kfir M, Arbel Y, et al. Lack of
682 interleukin-1alpha or interleukin-1beta inhibits transformation of steatosis to steatohepatitis
683 and liver fibrosis in hypercholesterolemic mice. J Hepatol. 2011;55(5):1086-94.
684 23. Tandon P, Abrams ND, Carrick DM, Chander P, Dwyer J, Fuldner R, et al. Metabolic
685 Regulation of Inflammation and Its Resolution: Current Status, Clinical Needs, Challenges,
686 and Opportunities. J Immunol. 2021;207(11):2625-30.
687 24. O'Neill LA, Kishton RJ, Rathmell J. A guide to immunometabolism for immunologists.
688 Nat Rev Immunol. 2016;16(9):553-65.
689 25. Lauterbach MA, Hanke JE, Serefidou M, Mangan MSJ, Kolbe CC, Hess T, et al. Toll-
690 like Receptor Signaling Rewires Macrophage Metabolism and Promotes Histone Acetylation
691 via ATP-Citrate Lyase. Immunity. 2019;51(6):997-1011 e7.

692 26. Langston PK, Nambu A, Jung J, Shibata M, Aksoylar HI, Lei J, et al. Glycerol
693 phosphate shuttle enzyme GPD2 regulates macrophage inflammatory responses. Nat Immunol.
694 2019;20(9):1186-95.
695 27. Meoli L, Gupta NK, Saeidi N, Panciotti CA, Biddinger SB, Corey KE, et al.
696 Nonalcoholic fatty liver disease and gastric bypass surgery regulate serum and hepatic levels
697 of pyruvate kinase isoenzyme M2. Am J Physiol Endocrinol Metab. 2018;315(4):E613-E21.
698 28. Xu F, Guo M, Huang W, Feng L, Zhu J, Luo K, et al. Annexin A5 regulates hepatic
699 macrophage polarization via directly targeting PKM2 and ameliorates NASH. Redox Biol.
700 2020;36:101634.
701 29. Kong Q, Li N, Cheng H, Zhang X, Cao X, Qi T, et al. HSPA12A Is a Novel Player in
702 Nonalcoholic Steatohepatitis via Promoting Nuclear PKM2-Mediated M1 Macrophage
703 Polarization. Diabetes. 2019;68(2):361-76.
704 30. Das Gupta K, Shakespear MR, Curson JEB, Murthy AMV, Iyer A, Hodson MP, et al.
705 Class IIa Histone Deacetylases Drive Toll-like Receptor-Inducible Glycolysis and Macrophage
706 Inflammatory Responses via Pyruvate Kinase M2. Cell Rep. 2020;30(8):2712-28 e8.
707 31. Park SY, Kim JS. A short guide to histone deacetylases including recent progress on
708 class II enzymes. Exp Mol Med. 2020;52(2):204-12.
709 32. Narita T, Weinert BT, Choudhary C. Functions and mechanisms of non-histone protein
710 acetylation. Nat Rev Mol Cell Biol. 2019;20(3):156-74.
711 33. Friedmann DR, Marmorstein R. Structure and mechanism of non-histone protein
712 acetyltransferase enzymes. FEBS J. 2013;280(22):5570-81.
713 34. Martin M, Kettmann R, Dequiedt F. Class IIa histone deacetylases: regulating the
714 regulators. Oncogene. 2007;26(37):5450-67.
715 35. Das Gupta K, Shakespear MR, Iyer A, Fairlie DP, Sweet MJ. Histone deacetylases in
716 monocyte/macrophage development, activation and metabolism: refining HDAC targets for
717 inflammatory and infectious diseases. Clin Transl Immunology. 2016;5(1):e62.
718 36. Shakespear MR, Halili MA, Irvine KM, Fairlie DP, Sweet MJ. Histone deacetylases as
719 regulators of inflammation and immunity. Trends Immunol. 2011;32(7):335-43.
720 37. Wang Y, Abrol R, Mak JYW, Das Gupta K, Ramnath D, Karunakaran D, et al. Histone
721 deacetylase 7: a signalling hub controlling development, inflammation, metabolism and disease.
722 FEBS J. 2023;290(11):2805-32.
723 38. Kodikara IKM, Pflum MKH. Scaffolding Activities of Pseudodeacetylase HDAC7.
724 ACS Chem Biol. 2025;20(2):248-58.

725 39. Ramnath D, Das Gupta K, Wang Y, Abrol R, Curson JEB, Lim J, et al. The histone
726 deacetylase Hdac7 supports LPS-inducible glycolysis and Il-1beta production in murine
727 macrophages via distinct mechanisms. J Leukoc Biol. 2022;111(2):327-36.
728 40. Das Gupta K, Ramnath D, von Pein JB, Curson JEB, Wang Y, Abrol R, et al. HDAC7
729 is an immunometabolic switch triaging danger signals for engagement of antimicrobial versus
730 inflammatory responses in macrophages. Proc Natl Acad Sci U S A. 2023;120(4):e2212813120.
731 41. Shakespear MR, Hohenhaus DM, Kelly GM, Kamal NA, Gupta P, Labzin LI, et al.
732 Histone deacetylase 7 promotes Toll-like receptor 4-dependent proinflammatory gene
733 expression in macrophages. J Biol Chem. 2013;288(35):25362-74.
734 42. Ovchinnikov DA, van Zuylen WJ, DeBats CE, Alexander KA, Kellie S, Hume DA.
735 Expression of Gal4-dependent transgenes in cells of the mononuclear phagocyte system labeled
736 with enhanced cyan fluorescent protein using Csf1r-Gal4VP16/UAS-ECFP double-transgenic
737 mice. J Leukoc Biol. 2008;83(2):430-3.
738 43. Baeck C, Wehr A, Karlmark KR, Heymann F, Vucur M, Gassler N, et al.
739 Pharmacological inhibition of the chemokine CCL2 (MCP-1) diminishes liver macrophage
740 infiltration and steatohepatitis in chronic hepatic injury. Gut. 2012;61(3):416-26.
741 44. Parker R, Weston CJ, Miao Z, Corbett C, Armstrong MJ, Ertl L, et al. CC chemokine
742 receptor 2 promotes recruitment of myeloid cells associated with insulin resistance in
743 nonalcoholic fatty liver disease. Am J Physiol Gastrointest Liver Physiol. 2018;314(4):G483-
744 G93.
745 45. Kitade H, Chen G, Ni Y, Ota T. Nonalcoholic Fatty Liver Disease and Insulin
746 Resistance: New Insights and Potential New Treatments. Nutrients. 2017;9(4).
747 46. Sharabi K, Tavares CD, Rines AK, Puigserver P. Molecular pathophysiology of hepatic
748 glucose production. Mol Aspects Med. 2015;46:21-33.
749 47. Hatting M, Tavares CDJ, Sharabi K, Rines AK, Puigserver P. Insulin regulation of
750 gluconeogenesis. Ann N Y Acad Sci. 2018;1411(1):21-35.
751 48. Rull A, Escola-Gil JC, Julve J, Rotllan N, Calpe-Berdiel L, Coll B, et al. Deficiency in
752 monocyte chemoattractant protein-1 modifies lipid and glucose metabolism. Exp Mol Pathol.
753 2007;83(3):361-6.
754 49. Kanda H, Tateya S, Tamori Y, Kotani K, Hiasa K, Kitazawa R, et al. MCP-1 contributes
755 to macrophage infiltration into adipose tissue, insulin resistance, and hepatic steatosis in
756 obesity. J Clin Invest. 2006;116(6):1494-505.
757 50. Petersen MC, Vatner DF, Shulman GI. Regulation of hepatic glucose metabolism in
758 health and disease. Nat Rev Endocrinol. 2017;13(10):572-87.

759 51. Ramnath D, Irvine KM, Lukowski SW, Horsfall LU, Loh Z, Clouston AD, et al.
760 Hepatic expression profiling identifies steatosis-independent and steatosis-driven advanced
761 fibrosis genes. JCI Insight. 2018;3(14).
762 52. Gwag T, Reddy Mooli RG, Li D, Lee S, Lee EY, Wang S. Macrophage-derived
763 thrombospondin 1 promotes obesity-associated non-alcoholic fatty liver disease. JHEP Rep.
764 2021;3(1):100193.
765 53. Hamada T, Fondevila C, Busuttil RW, Coito AJ. Metalloproteinase-9 deficiency
766 protects against hepatic ischemia/reperfusion injury. Hepatology. 2008;47(1):186-98.
767 54. Kim YS, Nam HJ, Han CY, Joo MS, Jang K, Jun DW, et al. Liver X Receptor Alpha
768 Activation Inhibits Autophagy and Lipophagy in Hepatocytes by Dysregulating Autophagy-
769 Related 4B Cysteine Peptidase and Rab-8B, Reducing Mitochondrial Fuel Oxidation.
770 Hepatology. 2021;73(4):1307-26.
771 55. Han HS, Kang G, Kim JS, Choi BH, Koo SH. Regulation of glucose metabolism from
772 a liver-centric perspective. Exp Mol Med. 2016;48(3):e218.
773 56. Agius L. Role of glycogen phosphorylase in liver glycogen metabolism. Mol Aspects
774 Med. 2015;46:34-45.
775 57. Zhang T, Wang S, Lin Y, Xu W, Ye D, Xiong Y, et al. Acetylation negatively regulates
776 glycogen phosphorylase by recruiting protein phosphatase 1. Cell Metab. 2012;15(1):75-87.
777 58. Ma J, Wei K, Liu J, Tang K, Zhang H, Zhu L, et al. Glycogen metabolism regulates
778 macrophage-mediated acute inflammatory responses. Nat Commun. 2020;11(1):1769.
779 59. Mihaylova MM, Vasquez DS, Ravnskjaer K, Denechaud PD, Yu RT, Alvarez JG, et
780 al. Class IIa histone deacetylases are hormone-activated regulators of FOXO and mammalian
781 glucose homeostasis. Cell. 2011;145(4):607-21.
782 60. Wang B, Moya N, Niessen S, Hoover H, Mihaylova MM, Shaw RJ, et al. A hormone-
783 dependent module regulating energy balance. Cell. 2011;145(4):596-606.
784 61. Hume DA. Applications of myeloid-specific promoters in transgenic mice support in
785 vivo imaging and functional genomics but do not support the concept of distinct macrophage
786 and dendritic cell lineages or roles in immunity. J Leukoc Biol. 2011;89(4):525-38.
787 62. McCubbrey AL, Allison KC, Lee-Sherick AB, Jakubzick CV, Janssen WJ. Promoter
788 Specificity and Efficacy in Conditional and Inducible Transgenic Targeting of Lung
789 Macrophages. Front Immunol. 2017;8:1618.
790 63. Kadier K, Niu T, Ding B, Chen B, Qi X, Chen D, et al. PROTAC-Mediated HDAC7
791 Protein Degradation Unveils Its Deacetylase-Independent Proinflammatory Function in
792 Macrophages. Adv Sci (Weinh). 2024;11(36):e2309459.

64. Poon EK, Liu L, Wu KC, Lim J, Sweet MJ, Lohman RJ, et al. A novel inhibitor of class IIa histone deacetylases attenuates collagen-induced arthritis. Br J Pharmacol. 2024;181(23):4804-21.

65. Guerriero JL, Sotayo A, Ponichtera HE, Castrillon JA, Pourzia AL, Schad S, et al. Class IIa HDAC inhibition reduces breast tumours and metastases through anti-tumour macrophages. Nature. 2017;543(7645):428-32.

66. Freese K, Seitz T, Dietrich P, Lee SML, Thasler WE, Bosserhoff A, et al. Histone Deacetylase Expressions in Hepatocellular Carcinoma and Functional Effects of Histone Deacetylase Inhibitors on Liver Cancer Cells In Vitro. Cancers (Basel). 2019;11(10).

67. Llewellyn BD. An improved Sirius red method for amyloid. J Med Lab Technol. 1970;27(3):308-9.

68. Kleiner DE, Brunt EM, Van Natta M, Behling C, Contos MJ, Cummings OW, et al. Design and validation of a histological scoring system for nonalcoholic fatty liver disease. Hepatology. 2005;41(6):1313-21.

69. Wang Z, Liu Q, Wang L, Gilbert RG, Sullivan MA. The Extraction of Liver Glycogen Molecules for Glycogen Structure Determination. J Vis Exp. 2022(180).

70. Suzuki Y, Lanner C, Kim JH, Vilardo PG, Zhang H, Yang J, et al. Insulin control of glycogen metabolism in knockout mice lacking the muscle-specific protein phosphatase PP1G/RGL. Mol Cell Biol. 2001;21(8):2683-94.

71. Livak KJ, Schmittgen TD. Analysis of relative gene expression data using real-time quantitative PCR and the 2(-Delta Delta C(T)) Method. Methods. 2001;25(4):402-8.

72. Dobin A, Davis CA, Schlesinger F, Drenkow J, Zaleski C, Jha S, et al. STAR: ultrafast universal RNA-seq aligner. Bioinformatics. 2013;29(1):15-21.

73. Law CW, Chen Y, Shi W, Smyth GK. voom: Precision weights unlock linear model analysis tools for RNA-seq read counts. Genome Biol. 2014;15(2):R29.

74. Robinson MD, Oshlack A. A scaling normalization method for differential expression analysis of RNA-seq data. Genome Biol. 2010;11(3):R25.

75. Robinson MD, McCarthy DJ, Smyth GK. edgeR: a Bioconductor package for differential expression analysis of digital gene expression data. Bioinformatics. 2010;26(1):139-40.

824 ## Figure Legends:

825 **Figure 1. Myeloid *Hdac7* overexpression promotes expression of inflammatory genes in**
826 **the liver.**
827 mRNA levels of *Hdac7* (A), *Ccl2* (B), *Il1b* (C) and *Mmp9* (D) in livers from 9-22 wk old
828 MacHDAC7 and control MacBlue mice fed a chow diet. Data (normalised to *Hprt*) represent
829 mean ± SEM from n=12 mice (6 female and 6 male) for each group. Statistical significance
830 was determined by Student's *t*-test (ns, not significant; * p <0.05).
831
832 **Figure 2. Effect of myeloid *Hdac7* overexpression on body weight gain in mice fed a chow**
833 **versus HFHCHS diet.**
834 8-10 wk old male MacBlue and MacHDAC7 mice were fed a chow diet (chow, n=6 per group)
835 or a high fat, high cholesterol and high sucrose diet (HFHCHS, n=14-15 per group) for 24 wk.
836 A. Weekly body weight. B. Average weight gain in mice fed a HFHCHS versus chow diet,
837 calculated by substracting the average body weight of mice fed the chow diet from that of mice
838 fed the HFHCHS. Data shown are mean ± SEM of n=6 (chow) or n=14-15 (HFHCHS) mice
839 per group. Statistical analyses were perfomed using linear regression to compare the difference
840 in body weight between MacBlue and MacHDAC7 mice fed on their respective diets or
841 HFHCHS-induced weight gain (** p <0.01; **** p <0.0001). C. Fat and lean mass measured
842 by EchoMRI at wk 23. D-G. Tissue weights of liver, epididymal white adipose tissue (WAT),
843 kidney and spleen at wk 24. Data shown are mean ± SEM of n=6 (chow) or n=14 (HFHCHS)
844 mice and were analysed using repeated measures (C) or ordinary (D-G) two-way ANOVA
845 followed by Sidak's multiple comparison (ns, not significant; * p <0.05; ** p <0.01; **** p
846 <0.0001).
847
848 **Figure 3. Myeloid *Hdac7* overexpression drives hepatic inflammation but not steatosis.**
849 Hepatic mRNA levels of genes encoding inflammatory mediators and serum CCL2 levels in
850 male MacBlue and MacHDAC7 mice fed a chow or HFHCHS diet. A-B. Liver mRNA levels
851 of *Ccl2* (A) and *Il1b* (B) relative to *Hprt* were measured by RT-qPCR. C. CCL2 levels in mouse
852 serum were measured by ELISA. D. Representative H&E staining of livers from chow- or
853 HFHCHS-fed MacBlue and MacHDAC7 mice. Photos were acquired at 40 x magnification,
854 scale bar: 100 µm. Large lipid droplets (black arrows) and small lipid droplets (blue arrows)
855 and a focus of inflammation within the lobule (red arrows). E-I. Quantification of lobular
856 inflammation (E), lipid droplet counts (F-G), steatosis (H) and NAFLD activity score (I), as
857 per the NASH clinical research network scoring system after H&E staining. Data represent
858 mean ± SEM of n=6 (chow) or n=14 (HFHCHS) mice for each treatment group and were

859 analysed using Student's *t*-test (A-B) or two-way ANOVA followed by Sidak's multiple
860 comparison (C, E-I) (ns, not significant; * $p< 0.05$; ** $p< 0.01$; *** $p< 0.001$; **** $p< 0.0001$).
861
862 **Figure 4. Myeloid *Hdac7* overexpression increases fasted blood glucose levels, glucose**
863 **dysregulation and glycogen metabolism in mice fed a HFHCHS diet.**
864 6 h fasted blood glucose levels of MacBlue and MacHDAC7 mice fed a chow (**A**) or HFHCHS
865 (**C**) diet. Glucose tolerance test (GTT) was performed at wk 12 (**B** and **D**). Data shown are
866 mean ± SEM of n=5-6 (chow) or n=15 (HFHCHS) mice for each group. AUC, area under curve
867 analysis. **E.** Liver glycogen quantification. At termination of the study, mice were fasted for 6
868 h and glycogen levels were quantified in snap-frozen livers. Data (mean ± SEM) represent n=6
869 (chow) or n=14 (HFHCHS) mice for each group. **F.** Insulin levels in the circulation. Circulating
870 insulin levels were measured before diet feeding (wk 0), at wk 4 and at end-point, after mice
871 were fasted for 6 h. Data are mean ± SEM of n=5-6 (chow) or n=14 (HFHCHS) mice for each
872 treatment group. Statistical analyses were performed using Student's *t*-test (**A-D, F** wk 0) or
873 two-way ANOVA followed by Sidak's multiple comparison (**B, D, E-F**) (ns, not significant; *
874 $p< 0.05$; ** $p< 0.01$; *** $p< 0.001$).
875
876 **Figure 5. Myeloid *Hdac7* deficiency reduced fasting blood glucose levels in mice fed a**
877 **HFHCHS diet.**
878 8-10 wk old male *Hdac7*$^{+/+}$ and *Hdac7*$^{-/-}$ mice were fed a HFHCHS diet for 36 wk. **A.** Fasted
879 blood glucose levels were measured at wk 0, 8, 14, 16 and 24. Data are mean ± SEM of n=12
880 mice for each group and were analysed using Student's *t*-test (ns, not significant; * $p < 0.05$;
881 **** $p < 0.0001$). Glucose tolerance test (GTT) at wk 14 and wk 32 (**B-C**) and insulin tolerance
882 test (ITT) at wk 19 and wk 34 (**D-E**). Data shown are mean ± SEM of n=12 mice/ group.
883 Statistical analyses were performed using repeated measures two-way ANOVA followed by
884 Sidak's multiple comparison. Area under curve (AUC) of GTTs and ITTs were analysed using
885 Student's *t*-test (ns, not significant; * $p < 0.05$; ** $p < 0.01$).
886
887 **Figure 6. Association of *HDAC7* mRNA expression with signatures of human CLD.**
888 **A.** mRNA levels of *HDAC7* in liver biopsies from patients with early (stages 0-2) versus
889 advanced (stages 3-4) of CLD was determined by RNAseq. Differentially expressed genes
890 were identified using edgeR with TMM normalisation and Benjamini-Hochberg method for
891 fdr correction. Data indicate mean ± SEM, n = 69 (circles = early stages and triangles =
892 advanced stages). **B-F.** Spatial transcriptomic profiling of liver tissues from MacBlue and
893 MacHDAC7 mice was performed using the 10x Genomics Xenium platform. Expression of

894 eCFP and HDAC7 mRNAs was used to identify hepatic myeloid cells expressing HDAC7
895 (CFP^+/$HDAC7^+$ cells). **B.** A heatmap showing the 53 differentially expressed genes in
896 CFP^+/$HDAC7^+$ macrophages from MacBlue versus MacHDAC7 livers. **C-F.** Spatial co-
897 expression analysis of *VCAN* (**C**), *THBS1* (**D**), *MMP9* (**E**) and *RAB8B* (**F**) in MacBlue and
898 MacHDAC7 livers. Data are representative of two independent tissue samples from litter-
899 matched male MacBlue and MacHDAC7 mice fed a chow diet.

FIGURE 1

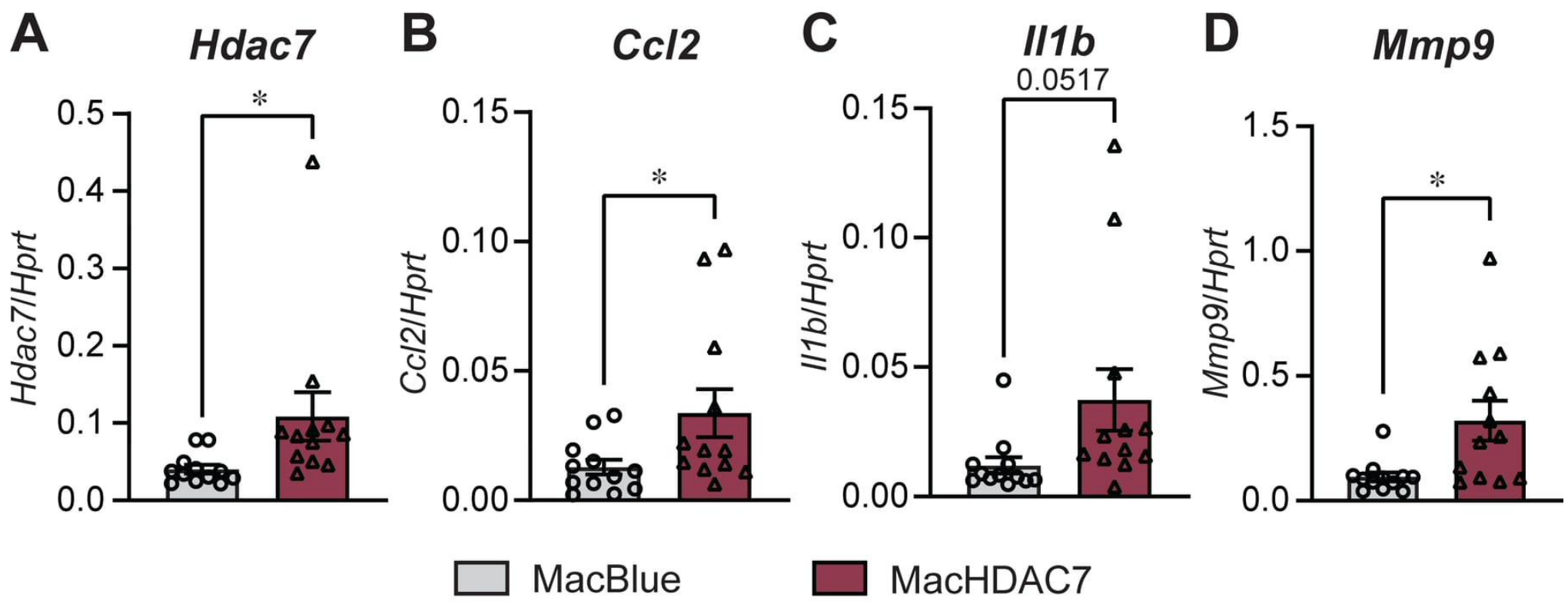
A
Hdac7
Hdac7/Hprt
0.5
0.4
0.3
0.2
0.1
0.0
*
B
Ccl2
Ccl2/Hprt
0.15
0.10
0.05
0.00
*
C
Il1b
0.0517
Il1b/Hprt
0.15
0.10
0.05
0.00
D
Mmp9
Mmp9/Hprt
1.5
1.0
0.5
0.0
*
MacBlue
MacHDAC7

FIGURE 2

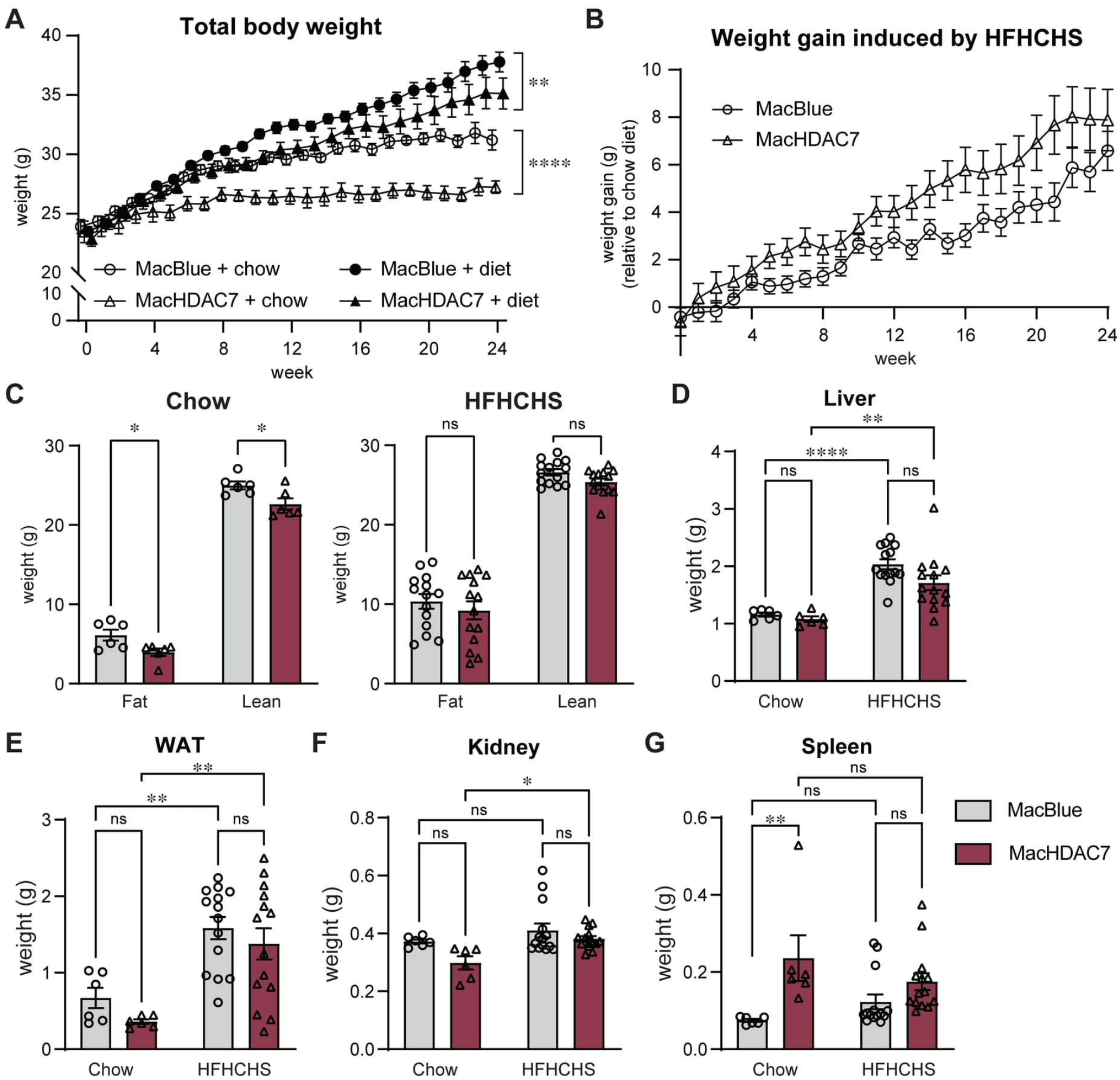
A
Total body weight
weight (g)
week
MacBlue + chow
MacHDAC7 + chow
MacBlue + diet
MacHDAC7 + diet
**
****
B
Weight gain induced by HFHCHS
weight gain (g)
(relative to chow diet)
week
MacBlue
MacHDAC7
**
C
Chow
HFHCHS
weight (g)
Fat
Lean
*
ns
D
Liver
weight (g)
Chow
HFHCHS
**
****
ns
E
WAT
weight (g)
Chow
HFHCHS
**
ns
F
Kidney
weight (g)
Chow
HFHCHS
*
ns
G
Spleen
weight (g)
Chow
HFHCHS
ns
**
MacBlue
MacHDAC7

FIGURE 3

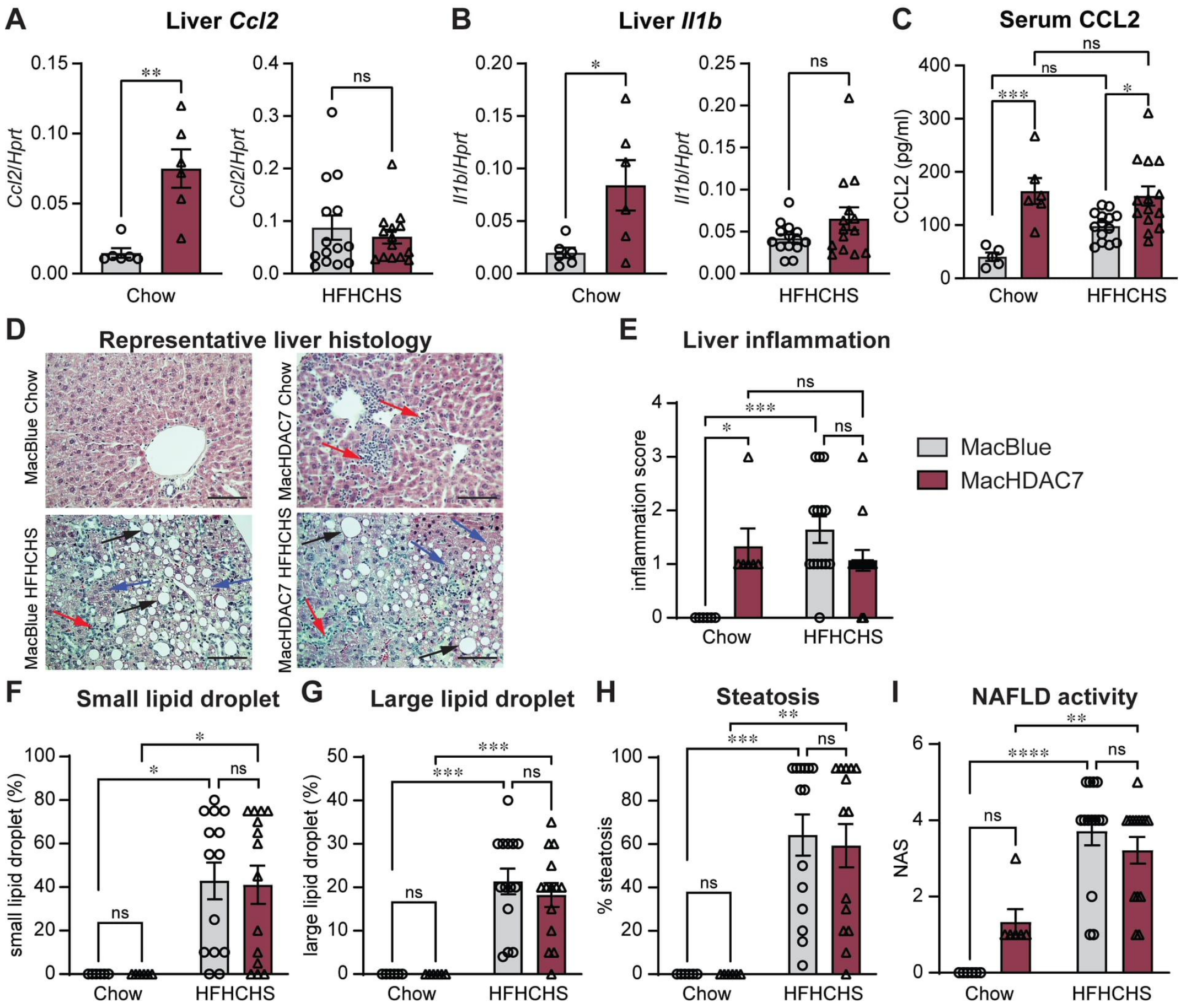
A
Liver Ccl2
Ccl2/Hprt
Chow
HFHCHS
B
Liver Il1b
Il1b/Hprt
C
Serum CCL2
CCL2 (pg/ml)
D
Representative liver histology
MacBlue Chow
MacHDAC7 Chow
MacBlue HFHCHS
MacHDAC7 HFHCHS
E
Liver inflammation
inflammation score
MacBlue
MacHDAC7
F
Small lipid droplet
small lipid droplet (%)
G
Large lipid droplet
large lipid droplet (%)
H
Steatosis
% steatosis
I
NAFLD activity
NAS

FIGURE 4

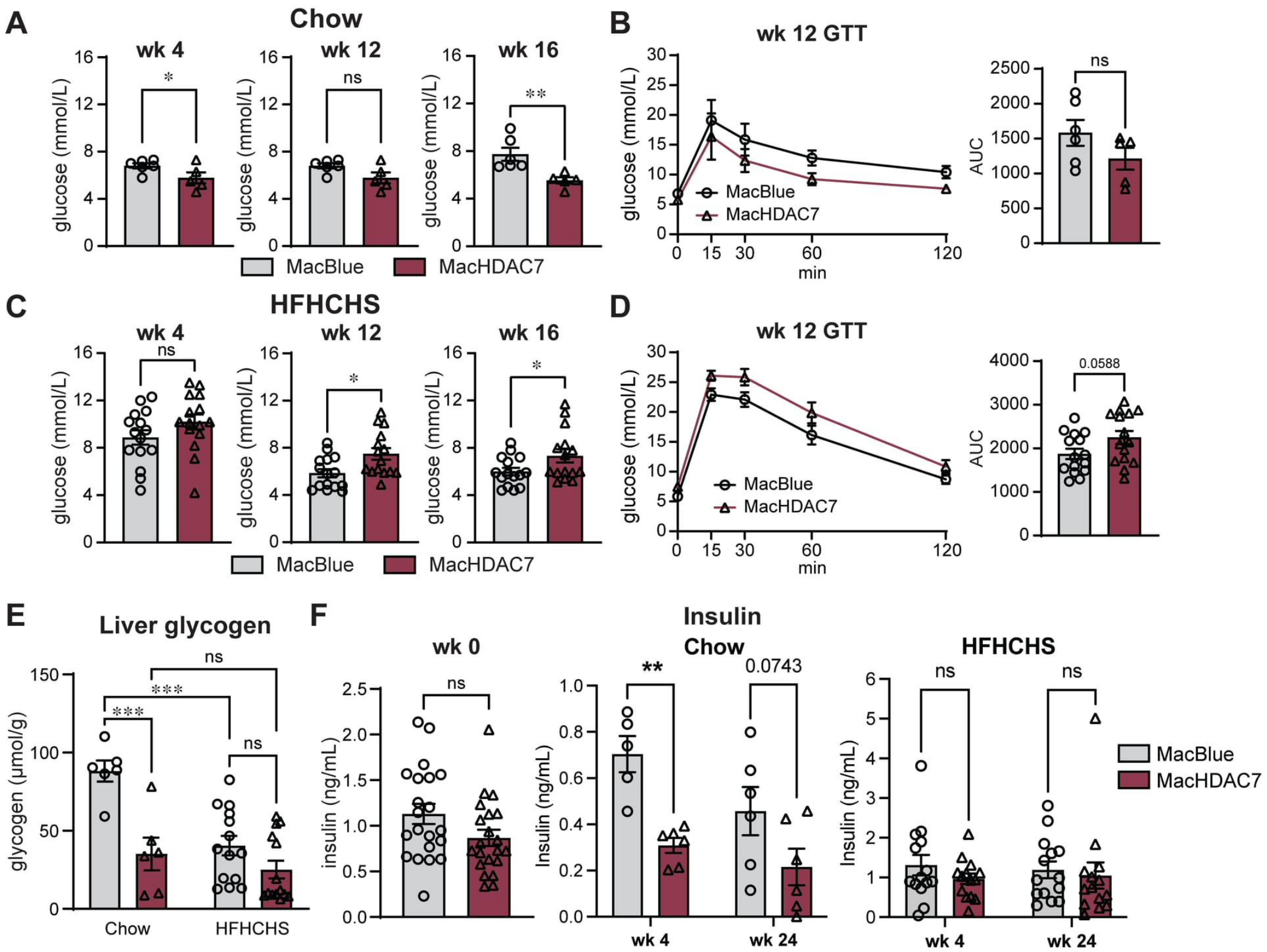
A
Chow
wk 4
wk 12
wk 16
glucose (mmol/L)
*
ns
**
MacBlue
MacHDAC7
B
wk 12 GTT
glucose (mmol/L)
MacBlue
MacHDAC7
min
AUC
ns
C
HFHCHS
wk 4
wk 12
wk 16
ns
*
*
D
wk 12 GTT
0.0588
E
Liver glycogen
glycogen (µmol/g)
***
***
ns
ns
Chow
HFHCHS
F
Insulin
wk 0
Chow
HFHCHS
insulin (ng/mL)
Insulin (ng/mL)
**
0.0743
ns
ns
wk 4
wk 24

FIGURE 5

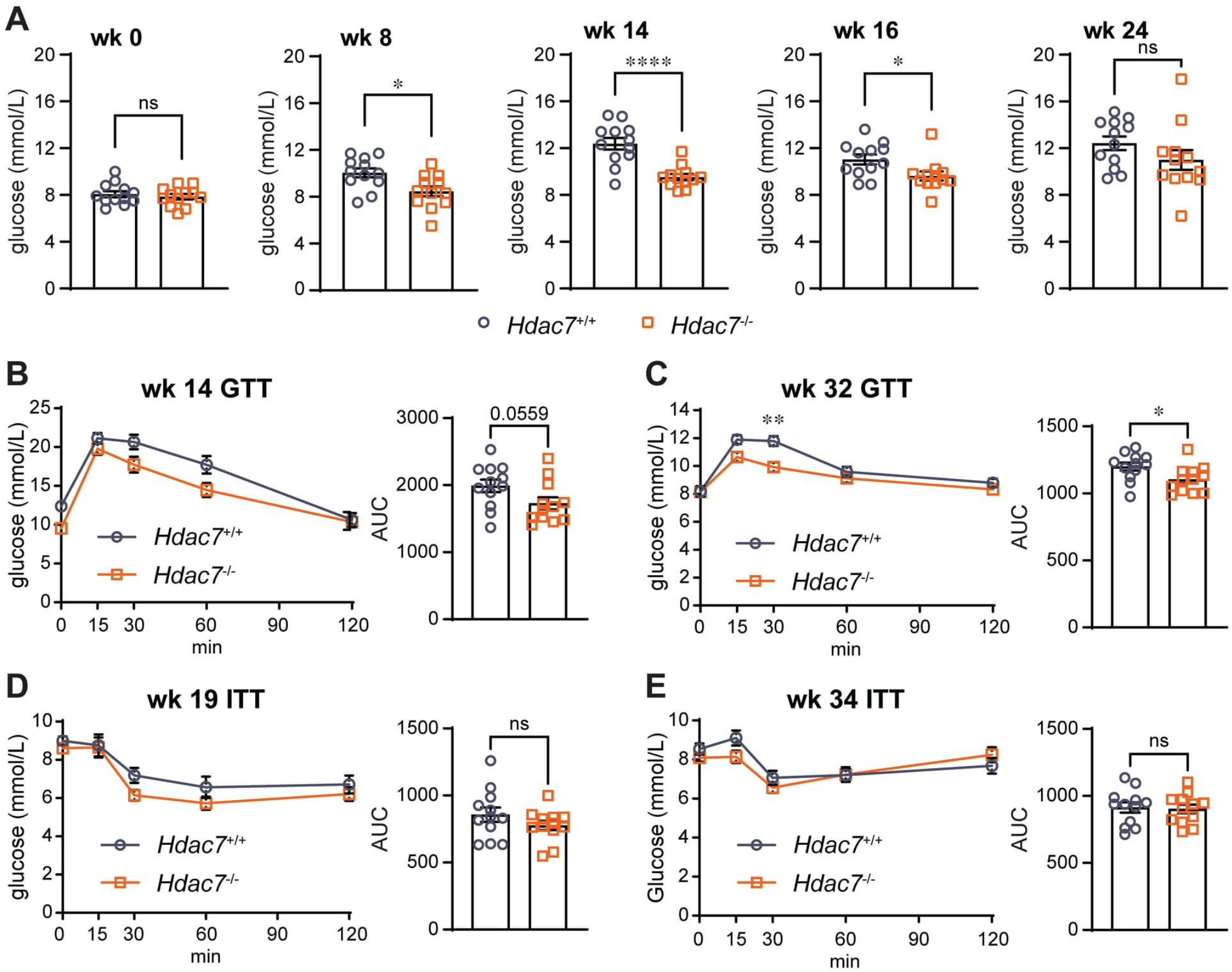
A
wk 0
wk 8
wk 14
wk 16
wk 24
glucose (mmol/L)
ns
*
****
*
ns
Hdac7+/+
Hdac7-/-
B
wk 14 GTT
glucose (mmol/L)
min
AUC
0.0559
C
wk 32 GTT
glucose (mmol/L)
min
AUC
**
*
D
wk 19 ITT
glucose (mmol/L)
min
AUC
ns
E
wk 34 ITT
Glucose (mmol/L)
min
AUC
ns

FIGURE 6

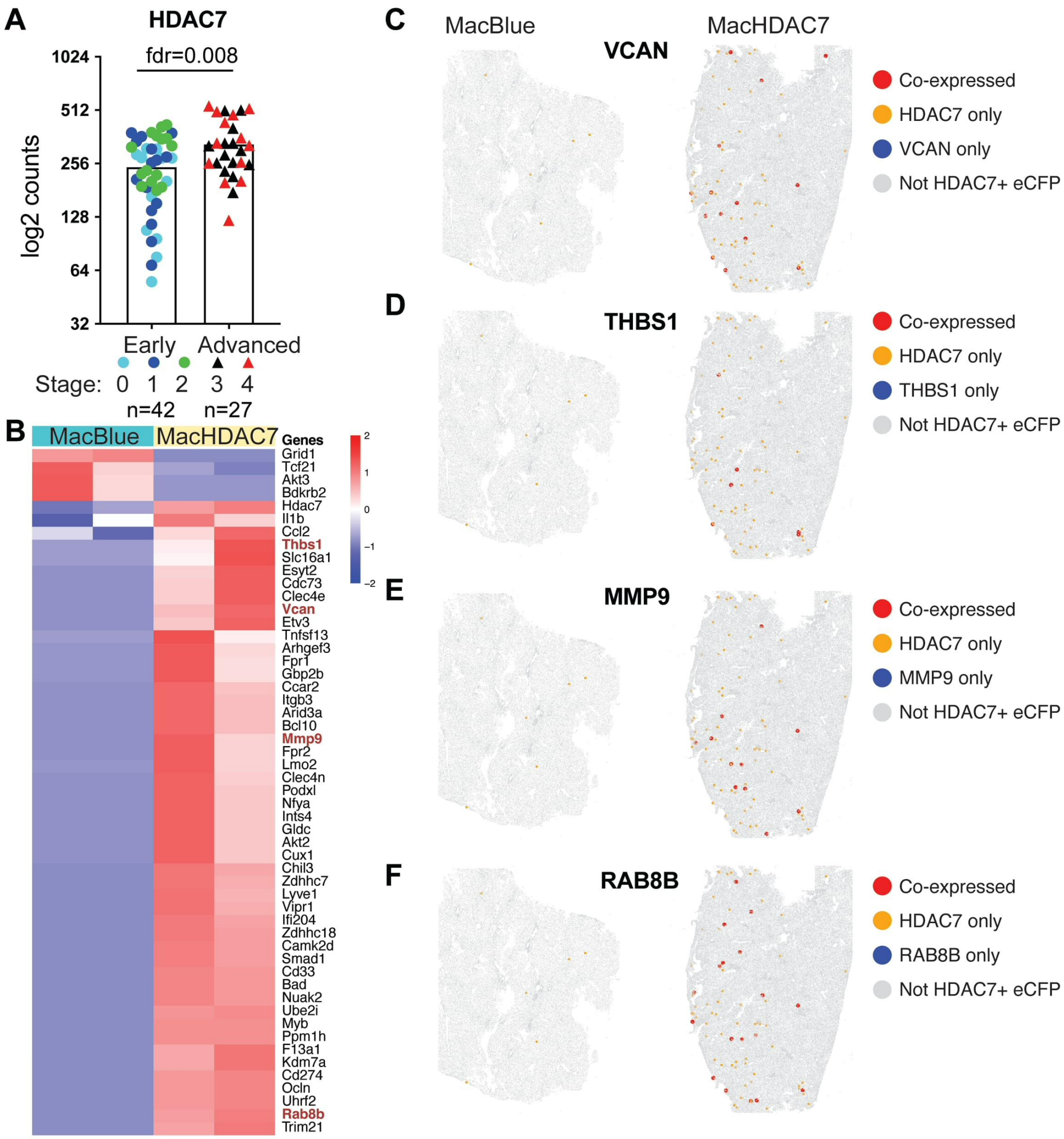
A
HDAC7
fdr=0.008
1024
512
256
128
64
32
log2 counts
Early
Advanced
Stage: 0 1 2 3 4
n=42 n=27
B
MacBlue
MacHDAC7
Genes
Grid1
Tcf21
Akt3
Bdkrb2
Hdac7
Il1b
Ccl2
Thbs1
Slc16a1
Esyt2
Cdc73
Clec4e
Vcan
Etv3
Tnfsf13
Arhgef3
Fpr1
Gbp2b
Ccar2
Itgb3
Arid3a
Bcl10
Mmp9
Fpr2
Lmo2
Clec4n
Podxl
Nfya
Ints4
Gldc
Akt2
Cux1
Chil3
Zdhhc7
Lyve1
Vipr1
Ifi204
Zdhhc18
Camk2d
Smad1
Cd33
Bad
Nuak2
Ube2i
Myb
Ppm1h
F13a1
Kdm7a
Cd274
Ocln
Uhrf2
Rab8b
Trim21
2
1
0
−1
−2
C
MacBlue
MacHDAC7
VCAN
Co-expressed
HDAC7 only
VCAN only
Not HDAC7+ eCFP
D
THBS1
Co-expressed
HDAC7 only
THBS1 only
Not HDAC7+ eCFP
E
MMP9
Co-expressed
HDAC7 only
MMP9 only
Not HDAC7+ eCFP
F
RAB8B
Co-expressed
HDAC7 only
RAB8B only
Not HDAC7+ eCFP

SUPPLEMENTARY INFORMATION

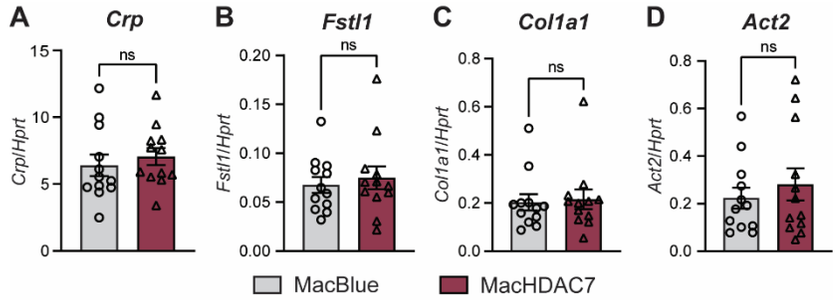

Supplementary Figure S1. Hepatic mRNA expression of inflammatory and fibrotic genes in MacHDAC7 mice.

Hepatic mRNA levels of inflammation marker *Crp* (**A**), and fibrotic markers *Fstl1* (**B**), *Col1a1* (**C**) and *Act2* (**D**) in livers from 9-22 wk old MacHDAC7 and control MacBlue mice fed a chow diet (same cDNA samples as used in Figure 1). Data, expressed relative to levels of *Hprt* mRNA, are mean ± SEM from n=12 mice (6 male and 6 female) for each group. Statistical analyses were performed using Student's *t*-test or (ns, not significant).

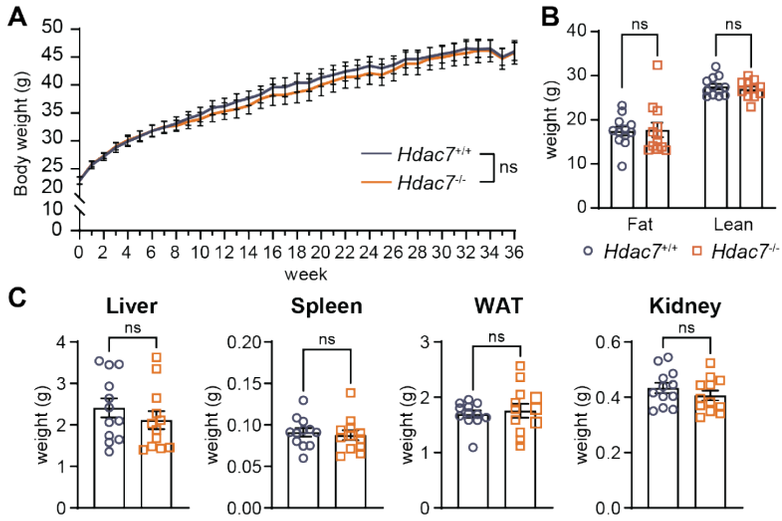

Supplementary Figure S2. Effect of myeloid *Hdac7* deletion on body weight in mice fed a chow versus HFHCHS diet.

8-10 wk old male *Hdac7*$^{fl/fl}$ (*Hdac7*$^{+/+}$) and *Hdac7*$^{fl/fl}$ *LysM*^{Cre} (*Hdac7*$^{-/-}$) mice were fed a HFHCHS diet for 36 wk. **A.** Body weight was measured weekly. **B.** Fat and lean mass measured by EchoMRI at wk 35. **C.** Total organ weights for liver, spleen, epididymal white adipose tissue (WAT) and kidney were measured at the termination of the study. Data shown are mean ± SEM of 12 mice from each group. Statistical analysis was performed using linear regression (**A**), repeated measures two-way ANOVA followed by Sidak's multiple comparison (**B**) or Student's *t*-test (**C**) (ns, not significant).

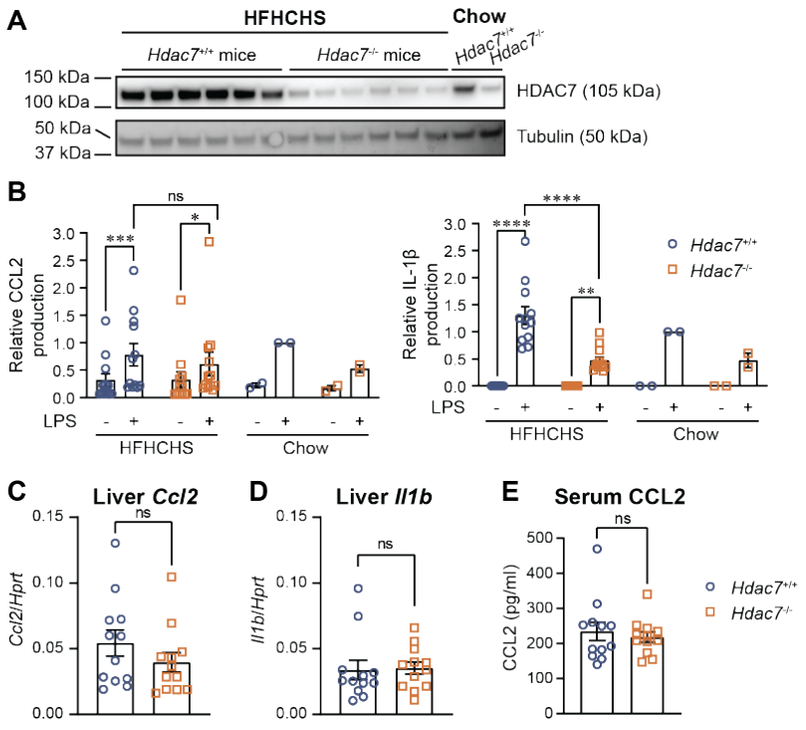

Supplementary Figure S3. Myeloid *Hdac7* deletion reduces inflammatory responses in macrophages but does not affect hepatic inflammatory gene expression or serum CCL2 in mice fed a HFHCHS diet.

A. Bone marrow cells from *Hdac7*$^{+/+}$ and *Hdac7*$^{-/-}$ mice on the HFHCHS diet were collected and differentiated in the presence of CSF-1 for 7 days and lysed, after which protein levels of HDAC7 were determined by immunoblotting, with Tubulin as a loading control (n=6 per group). BMMs from a pair of 12 wk old *Hdac7*$^{+/+}$ and *Hdac7*$^{-/-}$ mice on a chow diet were used as a positive control. **B.** Differentiated BMMs from mice of indicated genotypes on a HFHCHS diet were stimulated with LPS (0.5 ng/ml) for 4 h. CCL2 (left) and nigericin-induced IL-1β secretion (right) in culture supernatants were measured by ELISA (left hand side of graphs). BMMs from 12 wk old mice on a chow diet were used as inter-assay control (right hand side of graphs). Relative CCL2 and IL-1β production was normalised to the LPS-inducible production from BMMs of control *Hdac7*$^{+/+}$ mice on the chow diet. Data shown are mean ± SEM of 12 mice for each group and were analysed using repeated measures two-way ANOVA followed by Bonferroni's correction (* $p < 0.05$; *** $p < 0.001$; **** $p < 0.0001$). **C-E.** Quantification of inflammatory mediators in the liver and circulation. mRNA levels of *Ccl2* (**C**) and *Il1b* (**D**) (relative to *Hprt*) were measured from freshly homogenised frozen livers. CCL2 levels in mouse sera was measured by ELISA (**E**). Data shown are mean ± SEM from 12 mice for each group and were analysed using Student's *t*-test (ns, not significant).

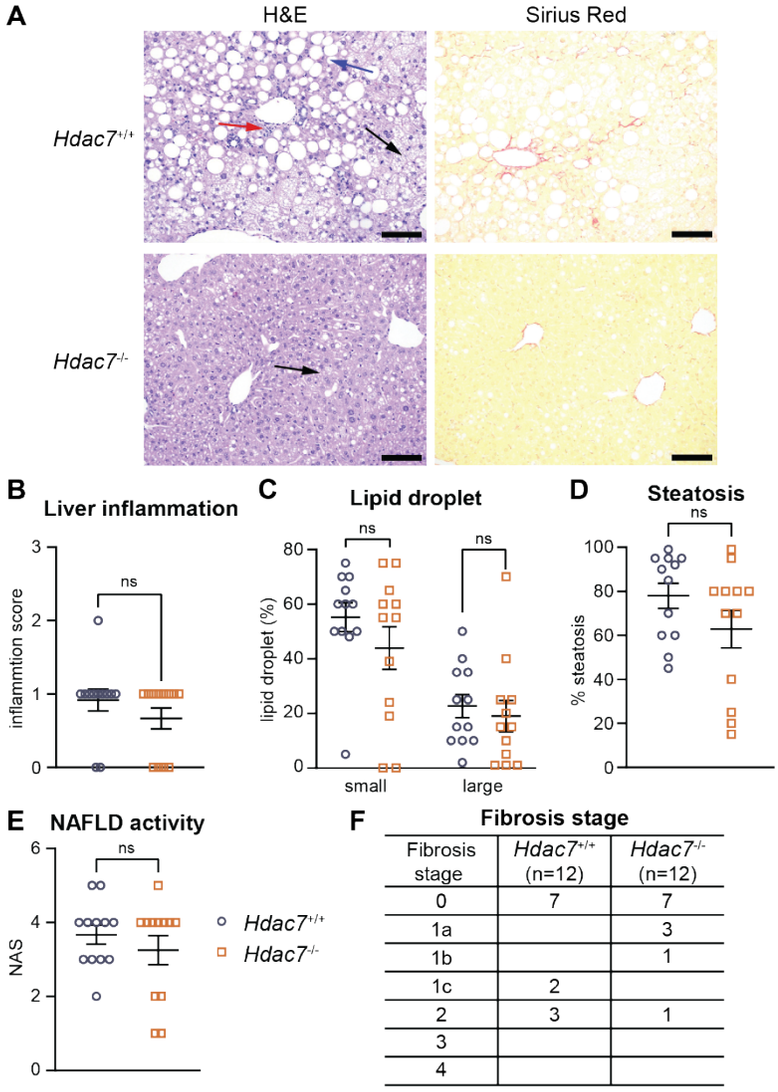

Fibrosis stage	*Hdac7*$^{+/+}$ (n=12)	*Hdac7*$^{-/-}$ (n=12)
0	7	7
1a		3
1b		1
1c	2	
2	3	1
3		
4		

Supplementary Figure S4. Histological assessment of livers from *Hdac7*$^{+/+}$ and *Hdac7*$^{-/-}$ mice. At termination of the study, mice were fasted for 12 h and euthanised. **A.** Liver pathology was assessed after H&E (left) and Siriud Red staining (right). Arrows indicate microvesicular steatosis (black), macrovesicular steatosis (blue), and a focus of inflammation within the lobule (red), scale bar: 100 µm. **B-F.** Quantification of lobular inflammation (**B**), lipid droplet counts (**C**), steatosis (**D**), NAFLD activity score (NAS, **E**) and fibrosis stage (**F**) as per the NASH clinical research network scoring system after H&E staining. Data shown represent mean ± SEM of 12 mice per group and were analysed using Student's *t*-test (**B**, **D-E**) or two-way ANOVA followed by Sidak's multiple comparison (**C**) (ns, not significant).

Supplementary Table S1. Fibrosis stage of livers from MacBlue and MacHDAC7 mice.

Fibrosis stage	Chow		HFHCHS	
	MacBlue (n=6)	MacHDAC7 (n=6)	MacBlue (n=14)	MacHDAC7 (n=14)
0	6	6	5	9
1a			3	3
1b			1	1
1c				
2			2	
3			3	1
4				

After H&E staining, fibrosis stage of livers from MacBlue and MacHDAC7 mice fed on the HFHCHS diet (from Figure 3) was scored according to the standards of NASH clinical research network scoring system. Numbers of mice at each stages of fibrosis is indicated in individual table cells.

Supplementary Table S2. Primer sequences used in this study.

Gene	Forward (5'-3')	Reverse (5'-3')
Hdac7	CGCAGCCAGTGTGAGTGTCT	AGTGGGTTCGTGCCGTAGAG
Ccl2	CCCACTCACCTGCTGCTACTCA	GCTTCTTTGGGACACCTGCTG
Il1b	GAAGTTGACGGACCCCAAAA	GCCTGCCTGAAGCTCTTGTT
Mmp9	TTGAGTCCGGCAGACAATCC	CCTTATCCACGCGAATGACG
Crp	GGCCAGATGCAAGCATCATC	CTGGAGATAGCACAAAGTCCCAC
Fstl1	CAACCCATCCTTCAACCCTCCT	ATTCTTTCCATCACAGGTCAT
Col1a1	CGTATCACCAAACTCAGAAG	GAAGCAAAGTTTCCTCCAAG
Act2	CATCTTTCATTGGGATGGA	TTAGCATAGAGATCCTTCCTG
Hprt	GTTGGATACAGGCCAGACTTTGTTG	GAGGGTAGGCTGGCCTATAGGCT